

**Dynamic Response and Maneuvering Strategies of
a Hybrid Autonomous Underwater Vehicle in
Hovering**

by

Lauren Alise Cooney

S.B., Massachusetts Institute of Technology (2006)

Submitted to the Department of Mechanical Engineering
in partial fulfillment of the requirements for the degree of

Master of Science in Ocean Engineering

at the

MASSACHUSETTS INSTITUTE OF TECHNOLOGY

February 2009

© Massachusetts Institute of Technology 2009. All rights reserved.

Author
Department of Mechanical Engineering
January 16, 2009

Certified by
Franz S Hover
Assistant Professor
Thesis Supervisor

Accepted by
David E Hardt
Chairman, Department Committee on Graduate Theses

Report Documentation Page

Form Approved
OMB No. 0704-0188

Public reporting burden for the collection of information is estimated to average 1 hour per response, including the time for reviewing instructions, searching existing data sources, gathering and maintaining the data needed, and completing and reviewing the collection of information. Send comments regarding this burden estimate or any other aspect of this collection of information, including suggestions for reducing this burden, to Washington Headquarters Services, Directorate for Information Operations and Reports, 1215 Jefferson Davis Highway, Suite 1204, Arlington VA 22202-4302. Respondents should be aware that notwithstanding any other provision of law, no person shall be subject to a penalty for failing to comply with a collection of information if it does not display a currently valid OMB control number.

1. REPORT DATE FEB 2009		2. REPORT TYPE		3. DATES COVERED 00-00-2009 to 00-00-2009	
4. TITLE AND SUBTITLE Dynamic Response and Maneuvering Strategies of a Hybrid Autonomous Underwater Vehicle in Hovering				5a. CONTRACT NUMBER	
				5b. GRANT NUMBER	
				5c. PROGRAM ELEMENT NUMBER	
6. AUTHOR(S)				5d. PROJECT NUMBER	
				5e. TASK NUMBER	
				5f. WORK UNIT NUMBER	
7. PERFORMING ORGANIZATION NAME(S) AND ADDRESS(ES) Massachusetts Institute of Technology, 77 Massachusetts Avenue, Cambridge, MA, 02139				8. PERFORMING ORGANIZATION REPORT NUMBER	
9. SPONSORING/MONITORING AGENCY NAME(S) AND ADDRESS(ES)				10. SPONSOR/MONITOR'S ACRONYM(S)	
				11. SPONSOR/MONITOR'S REPORT NUMBER(S)	
12. DISTRIBUTION/AVAILABILITY STATEMENT Approved for public release; distribution unlimited					
13. SUPPLEMENTARY NOTES					
14. ABSTRACT The Odyssey IV autonomous underwater vehicle (AUV) is the next generation of un-manned subsurface robots from the MIT Sea Grant AUV Laboratory. The Odyssey IV AUV has a novel propulsion system, which includes a pair of azimuthing thrusters for maneuvering in surge and heave. An analytical model was developed to describe the complex nonlinear vehicle dynamics, and experiments were performed to refine this model. The fluid dynamics of unsteady azimuthing marine propulsors are largely unstudied, especially for small vehicles like the Odyssey IV AUV. Experiments suggest that thrust developed by an azimuthing propulsor is dependent on the azimuth angle rate of change, and can substantially affect vehicle dynamics. A simple model capturing the effects of azimuthing on the thruster dynamics is developed, and is shown to improve behavior of the model. The use of azimuthing thrusters presents interesting problems and opportunities in maneuvering and control. Nonlinear model predictive control (MPC) is a technique that consists of the real-time optimization of a nonlinear dynamic system model, with the ability to handle constraints and nonlinearities. In this work, several variations of simulated and experimental MPC-based controllers are investigated. The primary challenge in applying nonlinear MPC to the Odyssey IV is solving the time intensive trajectory optimization problem online. Simulations suggest that MPC is able to capitalize on its knowledge of the system, allowing more aggressive trajectories than a traditional PID controller					
15. SUBJECT TERMS					
16. SECURITY CLASSIFICATION OF:			17. LIMITATION OF ABSTRACT	18. NUMBER OF PAGES	19a. NAME OF RESPONSIBLE PERSON
a. REPORT unclassified	b. ABSTRACT unclassified	c. THIS PAGE unclassified			

Dynamic Response and Maneuvering Strategies of a Hybrid Autonomous Underwater Vehicle in Hovering

by

Lauren Alise Cooney

Submitted to the Department of Mechanical Engineering
on January 16, 2009, in partial fulfillment of the
requirements for the degree of
Master of Science in Ocean Engineering

Abstract

The Odyssey IV autonomous underwater vehicle (AUV) is the next generation of unmanned subsurface robots from the MIT Sea Grant AUV Laboratory. The Odyssey IV AUV has a novel propulsion system, which includes a pair of azimuthing thrusters for maneuvering in surge and heave. An analytical model was developed to describe the complex nonlinear vehicle dynamics, and experiments were performed to refine this model. The fluid dynamics of unsteady azimuthing marine propulsors are largely unstudied, especially for small vehicles like the Odyssey IV AUV. Experiments suggest that thrust developed by an azimuthing propulsor is dependent on the azimuth angle rate of change, and can substantially affect vehicle dynamics. A simple model capturing the effects of azimuthing on the thruster dynamics is developed, and is shown to improve behavior of the model.

The use of azimuthing thrusters presents interesting problems and opportunities in maneuvering and control. Nonlinear model predictive control (MPC) is a technique that consists of the real-time optimization of a nonlinear dynamic system model, with the ability to handle constraints and nonlinearities. In this work, several variations of simulated and experimental MPC-based controllers are investigated. The primary challenge in applying nonlinear MPC to the Odyssey IV is solving the time intensive trajectory optimization problem online. Simulations suggest that MPC is able to capitalize on its knowledge of the system, allowing more aggressive trajectories than a traditional PID controller.

Thesis Supervisor: Franz S Hover
Title: Assistant Professor

Acknowledgments

First and foremost, I would like to thank my advisor, Professor Franz Hover, for providing me with guidance and encouragement throughout both my undergraduate and graduate careers. The members of the MIT AUV Lab past and present have built an awesome vehicle in the Odyssey IV AUV, and I appreciate all of their support. Justin Eskesen was an amazing source of knowledge regarding all things software. Thank you to the Department of Defense for providing me with a National Defense Science and Engineering Graduate (NDSEG) Fellowship, which has allowed me to dive into my interests. My office mates and the members of the Hover group provided interesting discussions. I want to thank Jordan Stanway for not only keeping me sane, but for also being an incredible source of knowledge and advice. Finally, I thank my family for their constant support and encouragement throughout my entire time at MIT.

Contents

1	Introduction	15
1.1	Motivation	15
1.2	Literature Review	17
1.2.1	Azimuthing Thrusters as Multi-Role Actuators	17
1.2.2	Discussion of Control Techniques	19
1.3	Problem Statement	22
1.3.1	Vehicle Description	22
1.3.2	Mission Scenarios	22
2	Vehicle Model	25
2.1	The Odyssey IV AUV	25
2.1.1	Vehicle Geometry	26
2.1.2	Vehicle Mass Properties	27
2.1.3	Propulsion	29
2.2	Equations of Motion	30
2.2.1	Coordinate Frames	30
2.2.2	Kinematics	31
2.2.3	Rigid Body Dynamics	32
2.2.4	Governing Equations of Motion	34
3	Hydrodynamic Coefficient Derivation	37
3.1	Added Mass	37
3.1.1	Body Added Mass	38

3.1.2	Thruster Added Mass	41
3.2	Drag and Lift	41
3.2.1	Strip-Theory	43
3.2.2	Additional Terms	45
3.3	Hydrostatics	46
3.4	Propulsion Model	47
3.5	Complete Hydrodynamic Terms	50
4	Complete Model and Testing	51
4.1	Combined Nonlinear Equations of Motion	51
4.2	Simplified Model	54
4.2.1	Linearized Equations of Motion	54
4.2.2	Decoupled Linear Model	55
4.3	Validation/Adjustment	55
4.3.1	Testing Description	55
4.3.2	Figures and Analysis	56
5	Controller Design	59
5.1	Algorithm Description	59
5.1.1	PID	59
5.1.2	Model Predictive Controller	62
6	Nonlinear Constrained Model Predictive Controller	67
6.1	Introduction	67
6.1.1	Problem Formulation	68
6.2	Optimization Methods	69
6.2.1	Methods	70
6.2.2	Performance	71
6.3	Controller Simulation and Experimental Results	71
6.3.1	PID Closed-Loop Simulation vs PID Closed-Loop Experiment	73
6.3.2	MPC Open-Loop Simulation vs PID Closed-Loop Experiment	73

6.3.3	MPC Open-Loop Simulation vs MPC Open-Loop Experiment	73
6.3.4	MPC-PID Hybrid	76
7	Conclusions	81
A	Vehicle Mass Table	83
B	Coefficient Matrix	85

List of Figures

1-1	The Odyssey IV AUV	16
1-2	DP System	17
1-3	F-22 Raptor Aircraft	18
1-4	Bluefin-21 AUV	18
1-5	Sentry AUV	19
1-6	Deep-Water Corals	23
2-1	Odyssey IV Internal Structure	25
2-2	Comparison Between Odyssey II and IV Class AUVs	27
2-3	Odyssey IV Side View	27
2-4	Odyssey IV Top View	28
2-5	Odyssey IV Front View	28
2-6	Rotating Thruster Unit	30
2-7	Odyssey IV Coordinate Frames	30
3-1	Odyssey IV Profile (XZ -plane and XY -plane)	39
3-2	Unsteady Thrust Model	49
4-1	Experimental Response to Forcing in Surge	57
4-2	Comparison between Measured and Predicted Vehicle Response	58
5-1	Structure of MOOS PID	60
5-2	Closed-Loop PID Response	61
5-3	Closed-loop PID Response: Commanded Thrust Vectors	62

6-1	Performance Comparison between Optimization Methods	72
6-2	Comparison between Closed-Loop PID Simulation and Experiment .	74
6-3	Comparison between Open-Loop MPC Simulation and Closed-Loop PID Experiment	75
6-4	Comparison between Open-Loop MPC Simulation and Experiment .	77
6-5	Comparison between RTU Commands and Measured Output	78
6-6	MPC-PID Hybrid Control Diagram	79
6-7	MPC-PID Hybrid Controller Performance	80

List of Tables

2.1	On-Board Sensors	26
2.2	Odyssey IV Geometry	29
2.3	Odyssey IV Mass Properties	29
3.1	Body Added Mass Coefficients	40
3.2	Thruster Added Mass Coefficients	41
6.1	Optimization performance comparison	71
A.1	Odyssey IV Detailed Mass Table	83

Chapter 1

Introduction

1.1 Motivation

Underwater vehicles have become indispensable tools in deep water operations, oceanography, port security, offshore oil and gas, archaeology, and cable laying and surveying. Underwater vehicles take many shapes, from manned submersibles that transport human pilots and passengers, towed sleds that pull sensors behind a surface vessel, remotely operated vehicles (ROVs) that are piloted by telepresence, autonomous underwater vehicles (AUVs) that act independently and use electric motor driven propulsion, and gliders which are also autonomous but are driven by buoyancy. The application of these vehicles is dependent on a wide range of considerations, including mission objectives, operating conditions, and budget. The Massachusetts Institute of Technology Sea Grant College Program Autonomous Underwater Vehicle Laboratory (MIT AUV Lab) has developed the Odyssey IV AUV (figure 1-1). Odyssey IV represents a departure from existing underwater vehicles, with hybrid characteristics combining the low-drag profile and surveying abilities of a traditional AUV, and the low-speed maneuverability of ROVs. The Odyssey IV is equipped with a novel propulsion system, featuring two cross-body thrusters and a pair of azimuthing thrusters that allow for both cruising and hovering capabilities in four degrees of freedom (4-DOF).

AUV design presents a range of technical challenges and tradeoffs. Sensors pro-

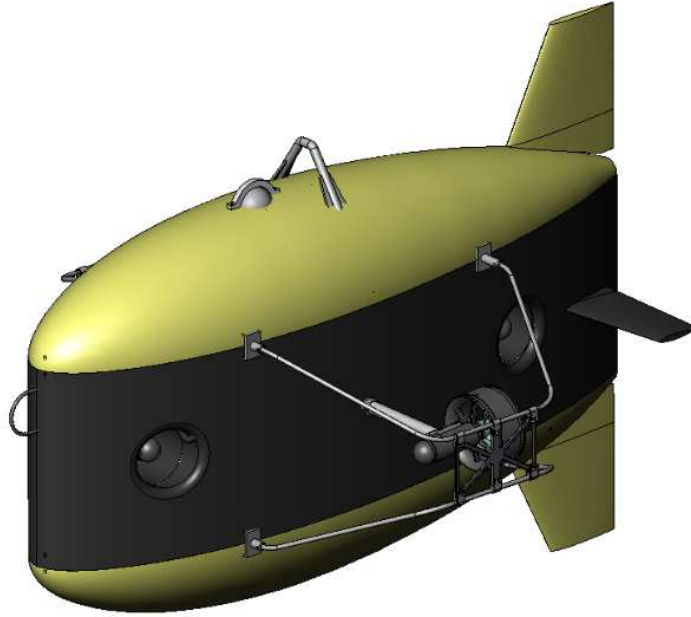


Figure 1-1: The Odyssey IV AUV from the MIT AUV Laboratory is a stream-lined vehicle with a pair of azimuthing thrusters and a pair of cross-body thrusters, for 4-DOF maneuvering even at zero-speed. The vehicle is rated for up to 6000m depth.

vide the tools to navigate and collect mission-specific data. Subsurface navigation is achieved using acoustic beacons and/or an on-board navigation suite of sensors. Power is generally provided by rechargeable batteries, and tradeoffs between cost and endurance are considered.

The traditional propulsion system of many AUVs is designed for long-transect survey missions. Forward thrust is provided by a single fixed propeller, and control surfaces generate the maneuvering forces required to steer the vehicle. This solution works well for a cruising vehicle, but the Odyssey IV AUV also has hovering mission requirements, and the traditional propulsion system does not allow for maneuvers at very low speeds [27].

Hovering is generally achieved using multiple thrusters distributed around the body to produce a net force vector. The use of multiple thrusters reduces complexity in the control problem and improves failure tolerance. However, the use of azimuthing thrusters—rotating the propulsor to produce thrust in the desired direction—in lieu of multiple thrusters proves an attractive alternative due to lower drag profile and

improved maneuverability. There are also alternatives to propeller-driven propulsion, such as biomimetic thrusters and jet propulsion systems that can lead to increases in efficiency and maneuverability.

1.2 Literature Review

1.2.1 Azimuthing Thrusters as Multi-Role Actuators

The increased maneuverability offered by azimuthing thrusters makes them important in the dynamic positioning community [43, 73]. The use of thrust-vectoring in aircraft



Figure 1-2: The offshore support vessel Toisa Perseus (foreground) and deepwater drillship Discoverer Enterprise are both equipped with dynamic positioning (DP) systems. Image provided courtesy of (<http://www.nationmaster.com/encyclopedia/Drill-ship>)

has enhanced maneuverability by improving vehicle pitch dynamics and enabling flight at increased angle of attack. Most thrust-vectoring in aircraft is achieved by deflecting the exhaust stream of a turbofan (figure 1-3). Several AUVs have been equipped with a single stern-mounted vectored thruster (figure 1-4) [40, 1]. The most similar vehicle to Odyssey IV is the Sentry AUV at the Woods Hole Oceanographic Institute (WHOI) (figure 1-5). It uses two pairs of thrusters—one forward and another aft—for actuation in five degrees (surge, heave, roll, pitch, and yaw). The thrusters are mated to large control surfaces and rotate through 270 degrees of pitch.



Figure 1-3: The Lockheed Martin/Boeing F-22 Raptor aircraft has pitch-axis thrust-vectoring turbofans, with a range of ± 20 deg, which make the aircraft highly maneuverable [3]. Image provided courtesy of the Lockheed Martin Corporation (<http://www.lockheedmartin.com/products/f22/index.html>)



Figure 1-4: The Bluefin-21 AUV is quipped with a single stern-mounted vectored thruster to aid in maneuvers during cruising. Image provided courtesy of the Bluefin Robotics Corporation (www.bluefinrobotics.com/index.htm)



Figure 1-5: The Woods Hole Oceanographic Institute’s Sentry AUV is equipped with two pairs of thrusters mated to large control surfaces which can rotate through 270 degrees of pitch. Image provided courtesy of the Ocean Observatories Initiative Regional Scale Nodes Program at the University of Washington (www.ooi.ocean.washington.edu/cruise)

1.2.2 Discussion of Control Techniques

Control in AUVs

The challenges associated with designing controllers for AUVs include a highly nonlinear dynamic model and complex hydrodynamic effects. The majority of AUVs use classical controllers such as proportional-integral-derivative (PID). Yuh [85] and Craven [13] cite a range of advanced controllers used in AUVs, including adaptive, fuzzy, neural network, nonlinear, and sliding mode controllers.

Although linear control theory has advantages in its extensive theoretical background, AUVs may exhibit nonlinear behavior that produces degraded performance outside of the linearized regime. Model predictive control continuously updates its solution based upon current states. It can handle nonlinearities in the control problem, and directly enforces constraints. These properties make it an attractive solution to the AUV control problem. Several simulations of model predictive controllers for AUVs have been presented [37, 50, 70, 77]. Kwiesielewicz [37] demonstrated improved

performance over more traditional controllers such as a PID controller and an adaptive controller. Truong [77] focuses on improving computational speed of MPC for use on AUVs. Naeem et al [57] realized real-time MPC using a genetic algorithm (GA) to solve the optimization problem online, and verified their findings through experiments. They found that the GA would not be sufficient for systems with low sampling periods.

Jakuba [36] developed a linear control system for the Sentry AUV (figure 1-5) based upon a vehicle model linearized about nominally horizontal flight, assuming small foil angles and small vertical velocity. PID control was used for a combined pitch-depth model. The controller performed adequately for simulations and experiments in which the vehicle was operating within the nominal operating regime. However, in simulations at high angle of attack or demanding steep desired ramp changes in depth, the pitch performance is degraded due to the linearized mapping of the nonlinear configuration of the actuators for the linear controller. Jakuba concluded that a nonlinear approach would be beneficial, suggesting a method that includes trigonometric modulation of the control with a dependence on foil angle.

Underactuated and Nonholonomic Systems

Odyssey IV is considered to be underactuated, meaning it has fewer control inputs (thrust, azimuth angle) than degrees of freedom (surge, heave, pitch). Additionally, from a study of the controllability, the azimuthing thruster unit is considered to be a nonholonomic system [41, 72].

Azimuthing thrusters have been implemented in the dynamic positioning systems of marine vessels, and as an underactuated system this presents a relevant control problem. However, the majority of azimuthing thruster dynamic positioning methods use periodic time-varying feedback control laws [55, 62] which require a quasi-static approach. This requires the dynamic response of the vessel to be much slower than that of the azimuthing thruster action. When a vehicle has relatively fast response, as is the case for Odyssey IV, this approach performs poorly, as demonstrated by Hover [33]. Leonard [41] successfully demonstrated path planning and open-loop control

of an underactuated AUV using sinusoidal/periodic controls, however, it should be noted that this was not for the AUV with azimuthing thruster case.

Thrust Vectoring in Flight Controllers

Although the dynamic time scales for thrust-vectoring in aircraft/spacecraft controllers results in a different problem than that of marine vehicles, research in this field is applicable to the nonlinear control inputs and high maneuverability requirements of the Odyssey IV AUV. Several flight controllers have been tested on a ducted fan experimental setup developed by the California Institute of Technology (Caltech) [52]. Model predictive control (MPC), or receding horizon control (RHC), are of particular interest and have been applied to the control of high performance flight vehicles [18, 25, 51, 84].

The methodology of the Caltech flight controllers involves the on-line solution of an optimal control problem over a finite time horizon using a nonlinear programming software package (NTG, for nonlinear trajectory generation [52]). The general approach of trajectory generation involves mapping the equations of motion to a lower dimensional output space to decrease the complexity of the optimization problem, using differential flatness [79] or the lowest space possible [51]. The output of the optimization is then fit to a B-spline polynomial.

Controller performance is evaluated by simulation and experiments. Special attention must be placed on timing schemes and the formulation of the optimization problem. A warm start strategy, where the previous trajectory solution is applied as an initial guess in the optimization problem, should be used. Milam [51] presents a controller capable of achieving computational speeds faster than 10 Hz.

1.3 Problem Statement

1.3.1 Vehicle Description

The Odyssey IV has a unique propulsion system that allows for maneuvering in multiple degrees of freedom at near-zero speed. It also has a low drag profile which makes it well suited for cruising. The vehicle is relatively transportable and inexpensive compared to other AUVs of similar performance.

1.3.2 Mission Scenarios

The proposed mission scenario for the Odyssey IV AUV consists of short exploratory missions with fast descent and ascent. Each mission begins with a descent phase, aided by a streamline drop weight. The vehicle may be driving “blind” without position estimates due to exceeded Doppler Velocity Log (DVL) sensor range/limited bottom lock (see Table 2.1). The vehicle then performs surveys and/or cruises to a desired target where it will hover to perform a task. After all behaviors are performed, the ascent weight is dropped and the vehicle returns to the surface.

Deep-Water Corals

Odyssey IV is intended to be an exploratory vehicle. Its stream-lined shape enables it to perform surveys, from which other vehicles such as Alvin (WHOI) would then be able to perform more extensive tasks. Deep-water (or cold-water) corals are a growing field of study that is increasingly of interest, as they are indicators of climate change [2, 71]. At depths of up to 2000m, many of these reefs lay undiscovered. Using a larger human-operated vehicle such as Alvin (WHOI) to search is not cost-effective due to the limited availability, high operational cost, and slow descent/ascent. A partnership between the MIT AUV Lab and Jess Adkins at the California Institute of Technology has been formed for Odyssey IV deep-water corals research.



Figure 1-6: Deep-water corals can be found all over the globe at depths of up to 2000m, and are indicators of past climate change. Photo credit: Barbara Hecker. Image provided courtesy of the NOAA Coral Reef Information System (CoRIS) (<http://www.coris.noaa.gov/about/deep/>)

Autonomous Intervention

Sub-sea intervention on oil or gas wells is required in order to perform basic maintenance and repairs. In many instances, ROVs have replaced human divers in order to perform tasks in deep or hazardous conditions. AUVs were initially used as survey technologies, however, there is interest in developing AUVs with intervention abilities. Some vehicles, such as the ALIVE AUV [20], use underwater navigation systems to transit to a desired position, then switch to supervisory control via acoustic communication to perform tasks at the site. Many intervention vehicles are equipped with robotic arms and/or tools to perform operations such as manipulating valves.

The MIT AUV Lab has joined with the Chevron Corporation to develop Odyssey IV to perform inspection tasks for risers and pipelines on the sea floor. Future capabilities include docking and intervention at subsea structures.

Archaeology

The MIT Sea Grant AUV Lab has a history of archaeological exploration [14], which includes survey and inspection of archaeological sites in areas such as Italy and Kythira, Greece. AUVs can be used for mapping and photo/video survey. Previous missions have demonstrated a need for the ability to closely follow non-smooth bottoms as well as terrain-following and hovering capabilities [16]. The Odyssey IV AUV represents a new technology for exploration of archaeological sites.

Chapter 2

Vehicle Model

2.1 The Odyssey IV AUV

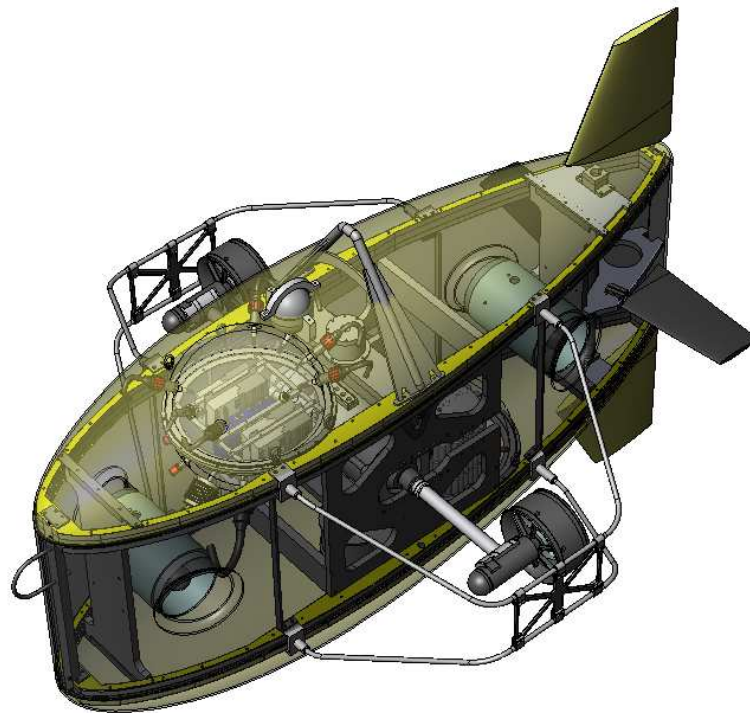


Figure 2-1: Odyssey IV Internal Structure

The MIT Sea Grant AUV Lab has developed the Odyssey IV, an exploratory autonomous underwater vehicle, designed for repeated rapid deployment, fast descent/ascent, and relatively short missions. It features two azimuthing thrusters for

motion in surge and heave, and two cross-body thrusters for maneuvering in yaw and sway. As of this writing, the Odyssey IV has been taken to depth of 50m and is currently designed for operation in up to 2500m deep water. Replacing several sensors increases the operational depth to 6000m.

The main vehicle computer consists of a PC-104 stack running a minimal installation of the Ubuntu operating system. Vehicle navigation and control is based on MOOS, a “Mission Oriented Operating Suite” [59]. A modified version named SGM OOS has been developed at the Sea Grant AUV Laboratory for use on their vehicles including Odyssey IV [19]. Navigation is achieved using a suite of integrated

Table 2.1: On-Board Sensors

Instrument	Measurement Application
Datasonics Sonar Altimeter	altitude
Harowe (DynaPar) Resolver	RTU position
Garmin GPS	position at the surface
Microstrain 3DM-GX1	angular velocity, acceleration, magnetic
Paroscientific Depth Sensor	depth
Teledyne Doppler Velocity Log (DVL)	velocity over the sea floor

sensors (Table 2.1), including an Inertial Navigation System (INS) and a Doppler Velocity Log (DVL), from which vehicle position during a mission is estimated using an Extended Kalman Filter.

2.1.1 Vehicle Geometry

The vehicle body is a modification of the Odyssey II Class AUV design (Figure 2-2). It is separated in the vertical direction for increased payload and improved roll/pitch stability

The streamlined shape is a modified foil section. The sides of the vehicle are faired, to make up an overall low drag profile for the hull. A pair of caged thrusters are offset from the vehicle. See figures 2-3: 2-5 for the vehicle schematic layout and Table 2.2 for the values of symbolic dimensions. Horizontal and vertical fins may be used for passive pitch and roll control at speed, as seen in figure 2-1, however, the

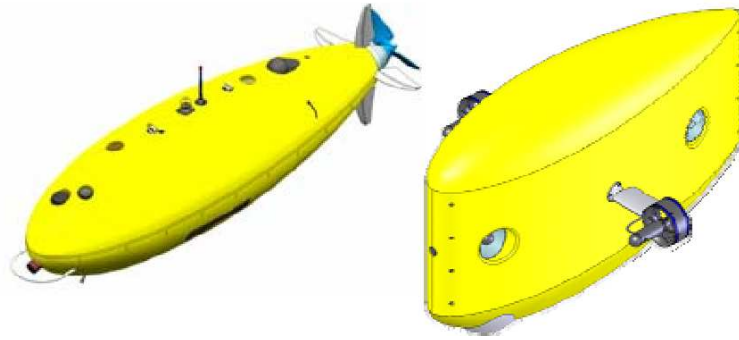


Figure 2-2: Comparison Between Odyssey II and IV Class AUVs

model and analysis presented in this thesis does not include them.

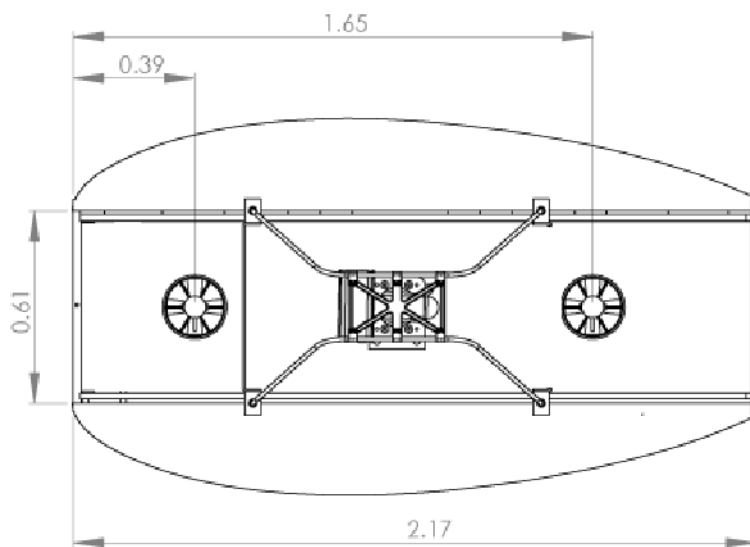


Figure 2-3: Odyssey IV Side View (dimensions in [m])

2.1.2 Vehicle Mass Properties

The vehicle and any entrained water within the flooded hull are modeled as a single rigid mass. The mass properties of the vehicle are described in Table 2.3. Refer to the vehicle mass table, Table A.1 in Appendix A, for the detailed positions of masses within the vehicle.

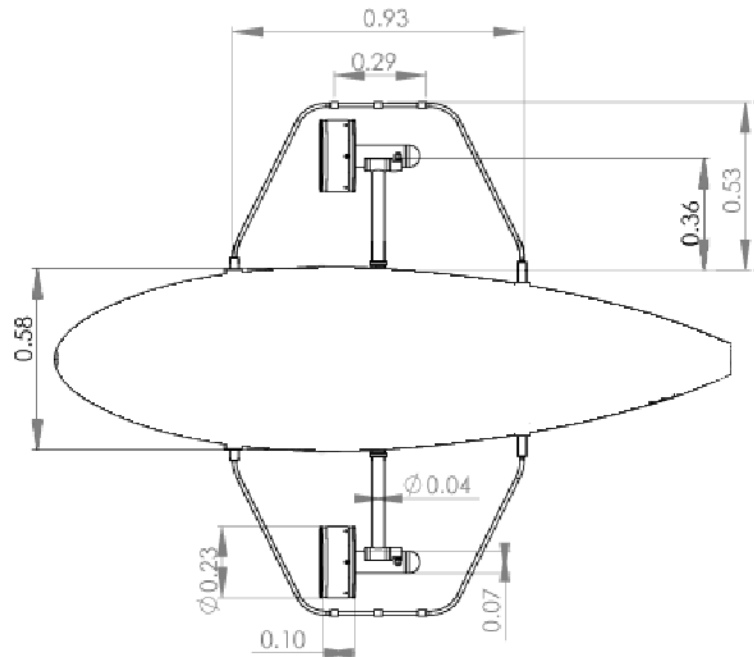


Figure 2-4: Odyssey IV Top View (dimensions in [m])

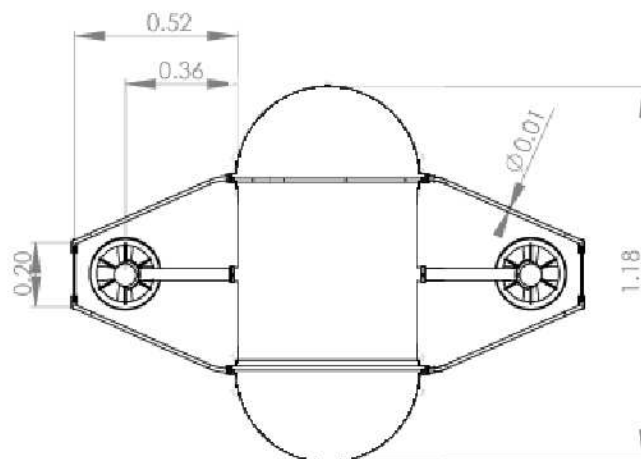


Figure 2-5: Odyssey IV Front View (dimensions in [m])

Table 2.2: Odyssey IV Geometry

Parameter	Value	Units	Description
L	2.17	m	body length
W	0.58	m	body width
H	1.19	m	body height

Table 2.3: Odyssey IV Mass Properties (All vectors referenced from the geometric origin of the body-fixed frame)

Parameter	Value	Units	Description
B	3345	N	body buoyancy force
m	339	kg	wet body mass
ρ	1000	kg*m ⁻³	density of water
x_G	0.01	m	x -vector to CG
y_G	0	m	y -vector to CG
z_G	0.00	m	z -vector to CG
x_B	0.02	m	x -vector to CB
y_B	0	m	y -vector to CB
z_B	-0.06	m	z -vector to CB
I_{xz}	4.1	kg*m ²	body product of inertia
I_x	55.5	kg*m ²	body moment of inertia
I_y	316.9	kg*m ²	body moment of inertia
I_z	290.7	kg*m ²	body moment of inertia

2.1.3 Propulsion

Odyssey IV's propulsion system provides 4 degree of freedom control. The vehicle uses four Deep Sea Systems TH-2100 thrusters. The thrusters are 7 inches in diameter, and produce 50 pounds of thrust at 1600 rpm. Two of the thrusters are tunneled, and configured cross-body for motion in sway and yaw. Another two of the thrusters are attached to a rotating unit, which can be rotated to provide the desired force vector in surge and heave (Figure 2-6). The rotating thruster unit (RTU) is driven by a servo drive for positioning control, has a resolver for positioning feedback, and moves independently through 360 degrees.

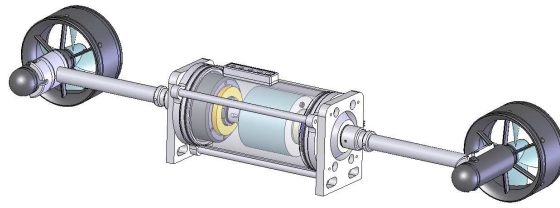


Figure 2-6: Rotating thruster unit (RTU) consisting of two independently azimuthed Deep Sea Systems TH-2100 thrusters

2.2 Equations of Motion

2.2.1 Coordinate Frames

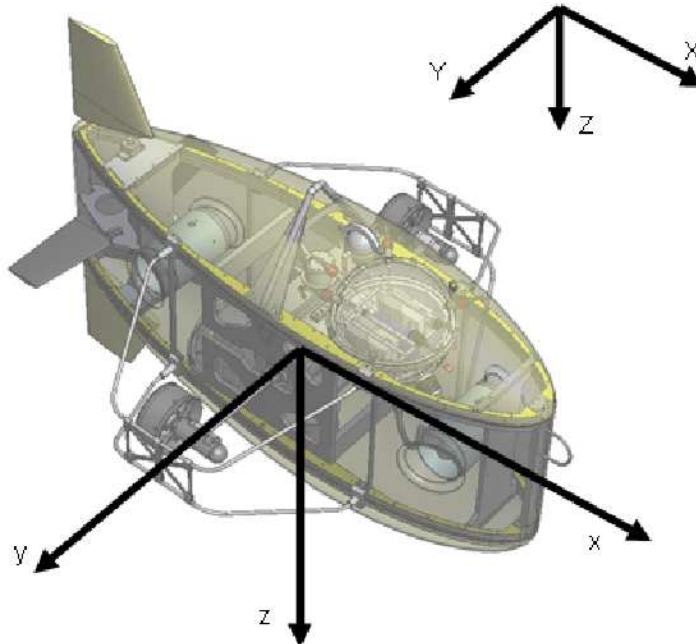


Figure 2-7: Odyssey IV inertial and body-fixed coordinate frames

Figure 2-7 illustrates the placement of the inertial and body-fixed coordinate frames. Vehicle motions are described relative to an inertial frame, which is fixed at the ocean surface. The body-fixed coordinate frame is positioned at the vehicle center of buoyancy, with x -axis forward, y -axis to starboard, and z -axis down. This placement yields both port-starboard and top-bottom symmetry, reducing the body's

inertia tensor \mathbf{I}_0 to:

$$\mathbf{I}_0 = \begin{bmatrix} I_x & 0 & I_{xz} \\ 0 & I_y & 0 \\ I_{xz} & 0 & I_z \end{bmatrix} \quad (2.1)$$

2.2.2 Kinematics

The motion of the vehicle in the inertial frame is described by the following vectors:

$$\begin{aligned} \boldsymbol{\eta} &= [\boldsymbol{\eta}_1^T, \boldsymbol{\eta}_2^T]^T; & \text{where } \boldsymbol{\eta}_1 &= [x, y, z]^T; \boldsymbol{\eta}_2 = [\phi, \theta, \psi]^T \\ \boldsymbol{\nu} &= [\boldsymbol{\nu}_1^T, \boldsymbol{\nu}_2^T]^T; & \text{where } \boldsymbol{\nu}_1 &= [u, v, w]^T; \boldsymbol{\nu}_2 = [p, q, r]^T \end{aligned}$$

where $\boldsymbol{\eta}$ refers to the inertial position and orientation vector, and $\boldsymbol{\nu}$ the body-fixed linear and angular velocities.

In order to transform linear velocities from body-fixed to inertial coordinate frames, we define the transformation matrix \mathbf{J}_1 , such that

$$\dot{\boldsymbol{\eta}}_1 = \mathbf{J}_1(\boldsymbol{\eta}_2)\boldsymbol{\nu}_1 \quad (2.2)$$

where

$$\mathbf{J}_1(\boldsymbol{\eta}_2) = \begin{bmatrix} c\phi c\psi - s\phi s\theta s\psi & -c\theta s\psi & s\phi c\psi + c\phi s\theta s\psi \\ c\phi s\psi + s\phi s\theta c\psi & c\theta c\psi & s\phi s\psi - c\phi s\theta c\psi \\ -c\theta s\phi & s\theta & c\phi c\theta \end{bmatrix} \quad (2.3)$$

where $c(\cdot)$ represents $\cos(\cdot)$ and $s(\cdot)$ represents $\sin(\cdot)$.

The transformation matrix \mathbf{J}_1 is generated by first performing a rotation of angle ψ about the z -axis, followed by a rotation of θ about the x -axis, and finally a rotation ϕ about the y -axis.

In order to determine the rotational velocities in the inertial frame there is a similar procedure which produces:

$$\dot{\boldsymbol{\eta}}_2 = \mathbf{J}_2(\boldsymbol{\eta}_2)\boldsymbol{\nu}_2 \quad (2.4)$$

where, using the same Euler angle sequence as above, \mathbf{J}_2 is defined as

$$\mathbf{J}_2(\boldsymbol{\eta}_2) = \frac{1}{c\theta} \begin{bmatrix} s\phi s\theta & c\theta & -c\phi s\theta \\ c\phi c\theta & 0 & c\theta s\phi \\ -s\phi & 0 & c\phi \end{bmatrix} \quad (2.5)$$

This matrix produces a singularity in roll, as opposed to the more traditional transformation matrices in Fossen [24] which produce a singularity in pitch. As Odyssey IV has high roll stability as well as the possibility of pitching due to the RTU or during fast descent, extreme angles in pitch are more likely to be of concern.

2.2.3 Rigid Body Dynamics

General Rigid Body Equations of Motion

The nonlinear equations of motion for a rigid body are developed by applying Newton's laws in the body-fixed coordinate frame, using the notation below:

$$\begin{aligned} \boldsymbol{\tau}_{RB} &= [\boldsymbol{\tau}_1^T, \boldsymbol{\tau}_2^T]^T; & \boldsymbol{\tau}_1 &= [X, Y, Z]^T; & \boldsymbol{\tau}_2 &= [K, M, N]^T \\ \mathbf{r}_G &= [x_G, y_G, z_G]^T \end{aligned}$$

where $\boldsymbol{\tau}_{RB}$ denotes external forces and moments acting on the vehicle with respect to the body-fixed frame, and \mathbf{r}_G the location of the vehicle center of gravity relative to the body-fixed frame. Following the methodology in Fossen [24] for deriving the inertial rigid body dynamics for a marine vehicle, the equations of motion are as

follows:

$$\begin{aligned}
m[\dot{u} + qw - rv + \dot{q}z_G - \dot{r}y_G + (qy_G + rz_G)p - (q^2 + r^2)x_G] &= \sum X_{ext} \\
m[\dot{v} + ru - pw + \dot{r}x_G - \dot{p}z_G + (rz_G + px_G)q - (r^2 + p^2)y_G] &= \sum Y_{ext} \\
m[\dot{w} + pv - qu + \dot{p}y_G - \dot{q}x_G + (px_G + qy_G)r - (p^2 + q^2)z_G] &= \sum Z_{ext} \\
I_x p + I_{xy} q + I_{xz} r + (I_z - I_y) r q + I_{yz} (q^2 - r^2) + I_{xz} p q - I_{xy} p r + \\
m[y_G (\dot{w} + pv - qu) - z_G (\dot{v} + ru - pw)] &= \sum K_{ext} \\
I_{yx} p + I_y q + I_{yz} r + (I_x - I_z) p r + I_{xz} (r^2 - p^2) + I_{xy} q r - I_{yz} q p + \\
m[z_G (\dot{u} + qw - rv) - x_G (\dot{w} + pv - qu)] &= \sum M_{ext} \\
I_{zx} p + I_{zy} q + I_z r + (I_y - I_x) p q + I_{xy} (p^2 - q^2) + I_{yz} p r - I_{xz} q r + \\
m[x_G (\dot{v} + ru - pw) - y_G (\dot{u} + qw - rv)] &= \sum N_{ext}
\end{aligned}$$

Using mass symmetry across the $x-z$ plane, the placement of the body-fixed frame at the vehicle center of buoyancy, and the simplified vehicle inertia tensor \mathbf{I}_0 as described in equation 2.1, the equations of motion are reduced to the following:

$$\begin{aligned}
m[\dot{u} + qw - rv + (\dot{q} + rp)z_G - (q^2 + r^2)x_G] &= \sum X_{ext} \\
m[\dot{v} + ru - pw + (pq + \dot{r})x_G + (rq - \dot{p})z_G] &= \sum Y_{ext} \\
m[\dot{w} + pv - qu + (pr - \dot{q})x_G - (p^2 + q^2)z_G] &= \sum Z_{ext} \\
I_x \dot{p} + I_{xz} r + (I_z - I_y) r q + I_{xz} p q - m[z_G (\dot{v} + ru - pw)] &= \sum K_{ext} \quad (2.6)
\end{aligned}$$

$$I_y \dot{q} + (I_x - I_z) p r + m[z_G (\dot{u} + qw - rv) - x_G (\dot{w} + pv - qu)] + \quad (2.7)$$

$$I_{xz} (r^2 - p^2) = \sum M_{ext}$$

$$\begin{aligned}
I_{zx} p + I_z \dot{r} + (I_y - I_x) p q - I_{xz} q r + m[x_G (\dot{v} + ru - pw)] &= \sum N_{ext} \\
& \quad (2.8)
\end{aligned}$$

Matrix Representation of Rigid-Body Equations of Motion

Following the representation of Fossen, the rigid-body equations of motion are expressed in matrix form as:

$$\mathbf{M}_{RB}\dot{\boldsymbol{\nu}} + \mathbf{C}_{RB}(\boldsymbol{\nu})\boldsymbol{\nu} = \boldsymbol{\tau}_{RB} \quad (2.9)$$

with rigid-body inertia matrix \mathbf{M}_{RB} and Coriolis and centripetal matrix \mathbf{C}_{RB} defined in (2.10) and (2.11) respectively.

$$\begin{aligned} \mathbf{M}_{RB} &= \begin{bmatrix} m\mathbf{I}_{3 \times 3} & -m\mathbf{S}(\mathbf{r}_G) \\ m\mathbf{S}(\mathbf{r}_G) & \mathbf{I}_0 \end{bmatrix} \\ &= \begin{bmatrix} m & 0 & 0 & 0 & 0 & mz_G & 0 \\ 0 & m & 0 & -mz_G & 0 & mx_G & 0 \\ 0 & 0 & m & 0 & -mx_G & 0 & 0 \\ 0 & -mx_G & 0 & I_x & 0 & 0 & -I_{xz} \\ mz_G & 0 & -mx_G & 0 & I_y & 0 & 0 \\ 0 & mx_g & 0 & -I_{zx} & 0 & I_z & 0 \end{bmatrix} \end{aligned} \quad (2.10)$$

$$\begin{aligned} \mathbf{C}_{RB} &= \begin{bmatrix} \mathbf{0}_{3 \times 3} & -m\mathbf{S}(\boldsymbol{\nu}_1) - m\mathbf{S}(\boldsymbol{\nu}_2)\mathbf{S}(\mathbf{r}_G) \\ -m\mathbf{S}(\boldsymbol{\nu}_1) + m\mathbf{S}(\mathbf{r}_G)\mathbf{S}(\boldsymbol{\nu}_2) & -\mathbf{S}(\mathbf{I}_0\boldsymbol{\nu}\boldsymbol{\nu}_2) \end{bmatrix} \\ &= \begin{bmatrix} 0 & 0 & 0 & mz+Gr & -m(x_Gq-w) & -m(x_Gr+v) \\ 0 & 0 & 0 & -mw & m(z_Gr+x_Gp) & mu \\ 0 & 0 & 0 & -m(z_Gp-v) & -m(z_Gq+u) & mx_Gp \\ -mz_Gr & mw & m(z_Gp-v) & 0 & -I_{xz}p+I_zr & -I_yq \\ m(x_Gq-w) & -m(z_Gr+x_Gp) & m(z_Gq+u) & I_{xz}p-I_zr & 0 & -I_{xz}r+I_xp \\ m(x_Gr+v) & -mu & -mx_Gp & I_yq & I_{xz}r-I_xp & 0 \end{bmatrix} \end{aligned} \quad (2.11)$$

where $\mathbf{I}_{3 \times 3}$ is the 3×3 identity matrix, \mathbf{I}_0 is the body's inertia tensor, and $\mathbf{S}(\boldsymbol{\lambda})$ is skew-symmetric matrix:

$$\mathbf{S}(\boldsymbol{\lambda}) = \begin{bmatrix} 0 & -\lambda_3 & \lambda_2 \\ \lambda_3 & 0 & -\lambda_1 \\ -\lambda_2 & \lambda_1 & 0 \end{bmatrix} \quad (2.12)$$

for unit vector $\boldsymbol{\lambda} = [\lambda_1, \lambda_2, \lambda_3]$.

2.2.4 Governing Equations of Motion

The total external forces and moments acting on the vehicle $\boldsymbol{\tau}_{RB}$ take into account $\boldsymbol{\tau}_{prop}$, the propulsion forces and moments, as well as $\boldsymbol{\tau}_H$, the effects due to the hydro-

dynamic forces and moments on the body:

$$\boldsymbol{\tau}_{RB} = \boldsymbol{\tau}_H + \boldsymbol{\tau}_{prop} \quad (2.13)$$

where $\boldsymbol{\tau}_H$ is defined as

$$\boldsymbol{\tau}_H = -\mathbf{M}_A \dot{\boldsymbol{\nu}} - \mathbf{C}_A(\boldsymbol{\nu})\boldsymbol{\nu} - \mathbf{D}(\boldsymbol{\nu})\boldsymbol{\nu} - \mathbf{g}(\boldsymbol{\eta}). \quad (2.14)$$

\mathbf{M}_A is the contribution from added mass, $\mathbf{C}_A(\boldsymbol{\nu})$ the added mass component of the Coriolis and centripetal component, $\mathbf{D}(\boldsymbol{\nu})$ the hydrodynamic lift and drag, and $\mathbf{g}(\boldsymbol{\eta})$ the hydrostatic restoring force. All hydrodynamic components are described more explicitly in Chapter 3.

Combining equations 2.13 and 2.14 with equation 2.9, the complete equations of motion as:

$$\mathbf{M}\dot{\boldsymbol{\nu}} + \mathbf{C}(\boldsymbol{\nu})\boldsymbol{\nu} + \mathbf{D}(\boldsymbol{\nu})\boldsymbol{\nu} + \mathbf{g}(\boldsymbol{\eta}) = \boldsymbol{\tau}_{prop} \quad (2.15)$$

$$\dot{\boldsymbol{\eta}} = \mathbf{J}(\boldsymbol{\eta})\boldsymbol{\nu} \quad (2.16)$$

where

$$\mathbf{M} = \mathbf{M}_{RB} + \mathbf{M}_A; \quad \mathbf{C}(\boldsymbol{\nu}) = \mathbf{C}_{RB}(\boldsymbol{\nu}) + \mathbf{C}_A(\boldsymbol{\nu});$$

Chapter 3

Hydrodynamic Coefficient Derivation

3.1 Added Mass

In fluid mechanics, an accelerating (or decelerating) body must move some volume of the surrounding fluid. Citing Newman [58], this volume of fluid is called the added mass, and for an ideal fluid, these forces and moments are defined as:

$$F_j = -\dot{u}_i m_{j,i} - \varepsilon_{jkl} u_i \Omega_k m_{l,i} \quad (3.1)$$

$$M_j = -\dot{u}_i m_{j+3,i} - \varepsilon_{jkl} u_i \Omega_k m_{l+3,i} - \varepsilon_{jkl} u_k \Omega_k m_{l,i} \quad (3.2)$$

where summation notion is implied and ε_{jkl} is the permutation symbol:

$$\begin{aligned} i &= 1, 2, 3, 4, 5, 6 \\ jkl &= 1, 2, 3 \\ \varepsilon_{jkl} &= \begin{cases} +1 & \text{if the indices are in cyclic order,} \\ -1 & \text{if the indices are in acyclic order,} \\ 0 & \text{if any pair of the indices are equal.} \end{cases} \end{aligned} \quad (3.3)$$

3.1.1 Body Added Mass

Due to the hull's top-bottom and port-starboard geometric symmetry, the hull added mass matrix simplifies to:

$$\mathbf{M}_{A_h} = - \begin{bmatrix} X_{\dot{u}_h} & 0 & 0 & 0 & 0 & 0 \\ 0 & Y_{\dot{v}_h} & 0 & 0 & 0 & N_{\dot{v}_h} \\ 0 & 0 & Z_{\dot{w}_h} & 0 & M_{\dot{w}_h} & 0 \\ 0 & 0 & 0 & K_{\dot{p}_h} & 0 & 0 \\ 0 & 0 & M_{\dot{w}_h} & 0 & M_{\dot{q}_h} & 0 \\ 0 & N_{\dot{v}_h} & 0 & 0 & 0 & N_{\dot{r}_h} \end{bmatrix} \quad (3.4)$$

$$\begin{aligned} X_A &= X_{\dot{u}}\dot{u} + Z_{\dot{w}}wq + Z_{\dot{q}}q^2 - Y_{\dot{v}}vr - Y_{\dot{r}}\dot{r}^2 \\ Y_A &= Y_{\dot{v}}\dot{v} + Y_{\dot{r}}\dot{r} + X_{\dot{u}}ur - Z_{\dot{w}}wp - Z_{\dot{q}}pq \\ Z_A &= Z_{\dot{w}}\dot{w} + Z_{\dot{q}}\dot{q} - X_{\dot{u}}uq + Y_{\dot{v}}vp + Y_{\dot{r}}rp \\ K_A &= K_{\dot{p}}\dot{p} \\ M_A &= M_{\dot{w}}\dot{w} + M_{\dot{q}}\dot{q} - (Z_{\dot{w}} - X_{\dot{u}})uw - Y_{\dot{r}}vp + (K_{\dot{p}} - N_{\dot{r}})rp - Z_{\dot{q}}uq \\ N_A &= N_{\dot{v}}\dot{v} + N_{\dot{r}}\dot{r} - (X_{\dot{u}} - Y_{\dot{v}})uv + Z_{\dot{q}}wp - (K_{\dot{p}} - M_{\dot{q}})pq + Y_{\dot{r}}ur \end{aligned} \quad (3.5)$$

Following Fossen [24], the axial added mass $X_{\dot{u}_h}$ of the hull can be estimated by approximating as an ellipsoid with major semi-axis a equal to the vehicle's maximum height and minor semi-axis b equal to the maximum body width. Fossen gives the lateral added mass of a prolate spheroid as:

$$X_{\dot{u}_h} = -\frac{4}{3}\rho ab^2 \frac{\beta_0}{2 - \beta_0} \quad (3.6)$$

where the constant β_0 is defined as:

$$\beta_0 = \frac{1}{e^2} - \frac{1 - e^2}{2e^3} \ln \frac{1 + e}{1 - e} \quad (3.7)$$

and eccentricity e defined as:

$$e = 1 - (b/a)^2 \quad (3.8)$$

The remaining added mass coefficients of the body are estimated using strip theory, in which the three-dimensional added mass coefficients are found by integrating the two-dimensional coefficients of the cross sections over the length of the appropriate body axis. Approximating the body as a series of elliptical cross-sections, Newman [58] gives the two-dimensional coefficients for an ellipse with major semi-axis a and minor semi-axis b as:

$$\begin{aligned} A_{22}^{(2D)}(y, z) &= \pi \rho b^2 \\ A_{33}^{(2D)}(y, z) &= \pi \rho a^2 \\ A_{44}^{(2D)}(y, z) &= \frac{1}{8} \pi \rho (a^2 - b^2)^2 \end{aligned}$$

The hull is approximated using the profiles shown in Figure 3-1. From these 2D added

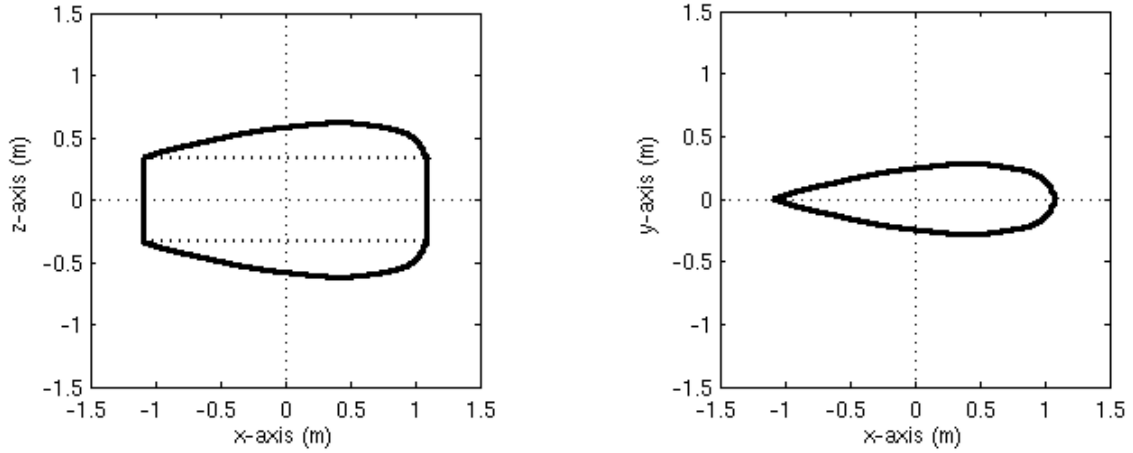


Figure 3-1: Odyssey IV Profile (XZ-plane and XY-plane)

mass coefficients, the three-dimensional values are as follows:

$$Y_{\dot{v}_h} = \pi\rho \int_{L_0^-}^{L_0^+} \left(\frac{1}{2}H_h(x)\right)^2 dx \quad (3.9)$$

$$Z_{\dot{w}_h} = \pi\rho \int_{L_0^-}^{L_0^+} \left(\frac{1}{2}W_h(x)\right)^2 dx \quad (3.10)$$

$$K_{\dot{p}_h} = \frac{1}{8}\pi\rho \int_{L_0^-}^{L_0^+} x \left(\left(\frac{1}{2}H_h(x)\right)^2 - \left(\frac{1}{2}W_h(x)\right)^2 \right) dx \quad (3.11)$$

$$M_{\dot{q}_h} = \pi\rho \int_{L_0^-}^{L_0^+} x^2 \left(\frac{1}{2}W_h(x)\right)^2 dx \quad (3.12)$$

$$N_{\dot{r}_h} = \pi\rho \int_{L_0^-}^{L_0^+} x^2 \left(\frac{1}{2}H_h(x)\right)^2 dx \quad (3.13)$$

$$M_{\dot{w}_h} = \pi\rho \int_{L_0^-}^{L_0^+} x \left(\frac{1}{2}W_h(x)\right)^2 dx \quad (3.14)$$

$$N_{\dot{v}_h} = \pi\rho \int_{L_0^-}^{L_0^+} x \left(\frac{1}{2}H_h(x)\right)^2 dx \quad (3.15)$$

where the terms $H_h(x)$ and $W_h(x)$ represent the hull height and width as a function of the hull length, and the limits of integration L_0^+ and L_0^- represent the longitudinal extent from the body origin to the vehicle nose and the body origin to the vehicle tail respectively.

Table 3.1: Body Added Mass Coefficients

Parameter	Value	Units
$X_{\dot{u}_h}$	-111.2	kg
$Y_{\dot{v}_h}$	-1994.3	kg
$Z_{\dot{w}_h}$	-300.5	kg
$K_{\dot{p}_h}$	-8.6	kg* m ²
$M_{\dot{q}_h}$	-75.3	kg* m ²
$N_{\dot{r}_h}$	-646.2	kg* m ²
$M_{\dot{w}_h}$	-74.7	kg* m
$N_{\dot{v}_h}$	-229.1	kg* m

3.1.2 Thruster Added Mass

The added mass due to the thrusters is quite complex. For simplicity, the outboard thrusters are modeled as cylinders (diameter 0.23m, length 0.29m) on cylindrical arms (diameter 0.04m, length 0.25m) offset from the vehicle. The added mass matrix due to the thrusters is defined as follows:

$$\mathbf{M}_{A_t} = - \begin{bmatrix} X_{\dot{u}_t} & 0 & 0 & 0 & M_{\dot{u}_t} & N_{\dot{u}_t} \\ 0 & Y_{\dot{v}_t} & 0 & K_{\dot{v}_t} & 0 & 0 \\ 0 & 0 & Z_{\dot{w}_t} & K_{\dot{w}_t} & 0 & 0 \\ 0 & K_{\dot{v}_t} & K_{\dot{w}_t} & K_{\dot{p}_t} & 0 & 0 \\ M_{\dot{u}_t} & 0 & 0 & 0 & M_{\dot{q}_t} & N_{\dot{q}_t} \\ N_{\dot{u}_t} & 0 & 0 & 0 & N_{\dot{q}_t} & N_{\dot{r}_t} \end{bmatrix} \quad (3.16)$$

Table 3.2: Thruster Added Mass Coefficients

Parameter	Value	Units
$X_{\dot{u}_t}$	-19.1	kg
$Y_{\dot{v}_t}$	-18.5	kg
$Z_{\dot{w}_t}$	-19.7	kg
$K_{\dot{p}_t}$	-8.2	kg* m ²
$M_{\dot{q}_t}$	-0.2	kg* m ²
$N_{\dot{r}_t}$	-7.8	kg* m ²
$K_{\dot{v}_t}$	0.5	kg* m
$K_{\dot{w}_t}$	3.8	kg* m
$M_{\dot{u}_t}$	-0.5	kg* m
$N_{\dot{u}_t}$	-4.8	kg* m
$N_{\dot{q}_t}$	-0.38	kg* m ²

3.2 Drag and Lift

Damping of underwater vehicle motions is coupled and nonlinear. A number of approximations are made in this work, in order to reduce complexity. For simplification of modeling, only first-order and second-order terms are considered.

The drag and lift forces are given by the following:

$$F_D = \frac{1}{2}\rho C_D(\alpha, R_e)Au|u| \quad (3.17)$$

$$F_L = \frac{1}{2}\rho C_L(\alpha, R_e)Au|u| \quad (3.18)$$

where A and u are characteristic area and velocities of the body, and drag coefficient C_D and lift coefficient C_L are functions of the angle of attack α and Reynolds number R_e . Reynolds number is the ratio of inertial to viscous forces, given by

$$R_e = \frac{uL}{\nu} \quad (3.19)$$

for characteristic length L and fluid kinematic viscosity ν , where ν is taken to be $1.19 \times 10^{-6} \text{m}^2/\text{s}$ at 15°C [58]. For the Odyssey IV, we are interested in both cruising and hovering operating ranges. In the interest of modeling, a range of operating speeds, estimated from 0.5m/s to 1.5m/s , give Reynolds numbers for a smooth surface from 0.9×10^6 to 2.7×10^6 . At higher speeds, the vehicle will be operating in the turbulent flow regime. At slower speeds, the vehicle is operating in the transitional regime between laminar and turbulent flow. However, the Odyssey IV hull is not entirely smooth, and turbulent flow is most likely to be tripped by the number of appendages/etc. A fully-developed turbulent, non-Reynolds number dependent approach is taken due to roughness, particles suspended in sea water, and the ambient turbulence of the ocean environment.

The objective is to find the nonlinear coefficients, for example, the axial drag coefficient $X_{u|u|}$:

$$X = \frac{1}{2}\rho C_D(\alpha, R_e)Au|u| = X_{u|u|}u|u| \quad (3.20)$$

Following the method developed by Jakuba [36], a strip-theory approach is used to determine the differential drag and lift of 2D sections due to the in-plane flow speed for that section, then integrating to find the total forces due to lift and drag. The longitudinal hull lift coefficients and drag forces due to the RTU are found using more traditional methods.

3.2.1 Strip-Theory

Coefficients

Leading coefficients are found using the simplified approaches used in [31, 32], using a linear approximation:

$$C_D \approx K_D \alpha \quad (3.21)$$

$$C_L \approx K_L \alpha \quad (3.22)$$

where K_D and K_L are the drag and lift coefficient slopes.

To determine drag coefficient of the body along the x -axis, the hull is approximated as a series of elliptical cross-sections, for which Hoerner [31] gives the equation for the 2D lateral drag coefficient $K_{D_{yz}}(x)$ as:

$$K_{D_{yz}}(x) = C_f \left(4 + 2 \frac{H(x)}{W(x)} + 120 \left(\frac{W(x)}{H(x)} \right)^2 \right) \quad (3.23)$$

where $H(x)$ and $W(x)$ represent the height and width of the vehicle body as a function of length, and C_f is the skin friction coefficient, taken to be $C_f=0.035$ for turbulent conditions [58]. Along the vertical axis z , the cross-sections are treated as small-aspect ratio wings, for which [31] gives the equation for the 2D longitudinal drag coefficient $K_{D_{xy}}(z)$ to be:

$$K_{D_{xy}}(z) = 2C_f \left(1 + 2 \frac{W(z)}{L(z)} + 60 \left(\frac{W(z)}{L(z)} \right)^4 \right) \quad (3.24)$$

The lift coefficient in the x -direction from [32] for a small aspect ratio wing is:

$$K_{L_{xy}} = \frac{\pi}{2} AR_x \quad (3.25)$$

where AR_x is the ratio of hull height to length.

Sectional Drag and Lift Forces

Using a strip theory approach, we find the sectional lift and drag forces caused by the local planar velocities. These can then be integrated over the body to find the forces and moments due to lift and drag. Considering the vehicle hull as a series of 2D cross-sections, the sectional quadratic drag force $d\mathbf{F}_D$ and lift force $d\mathbf{F}_L$ are given by the following:

$$d\mathbf{F}_D = \frac{1}{2}\rho C_D W(x_{2D}) \boldsymbol{\nu}_{2D}^T \boldsymbol{\nu}_{2D} dx_{2D} \quad (3.26)$$

$$d\mathbf{F}_L = \frac{1}{2}\rho C_L W(x_{2D}) \boldsymbol{\nu}_{2D}^T \boldsymbol{\nu}_{2D} dx_{2D} \quad (3.27)$$

where $W(x_{2D})$ is the characteristic width and $\boldsymbol{\nu}_{2D}$ the local planar velocity vector. For example, the sectional drag and lift forces in the xy -plane are:

$$d\mathbf{F}_{D,xy} = -\frac{1}{2}\rho K_{D_{xy}} b_{xy}(z) \boldsymbol{\nu}_{z,2D}^T \boldsymbol{\nu}_{z,2D} dz \quad (3.28)$$

$$d\mathbf{F}_{L,xy} = -\frac{1}{2}\rho K_{L_{xy}} b_{xy}(z) \boldsymbol{\nu}_{z,2D}^T \boldsymbol{\nu}_{z,2D} dz \quad (3.29)$$

Total Drag and Lift Forces

The total sectional planar force $d\mathbf{F}_{tot}$ is simply

$$d\mathbf{F}_{tot} = d\mathbf{F}_D + d\mathbf{F}_L. \quad (3.30)$$

This force acts at the center of pressure CP , which is located at $\frac{1}{4}$ chord from the leading edge for a thin foil [42], for which the moment arm to the body origin is defined as \mathbf{r}_{CP} . The differential moment is then defined as:

$$d\mathbf{M}_{tot} = \mathbf{r}_{CP} \times d\mathbf{F}_{tot} \quad (3.31)$$

the total forces can be found by integrating the sectional drag and lift forces onto the entire vehicle. For example, in the x and k directions, we find the total forces and

moments on the body due to drag and lift to be:

$$\begin{aligned}
X &= \int_{L_0^-}^{L_0^+} (d\mathbf{F}_D + d\mathbf{F}_L) dx_{2D} \\
K &= \int_{L_0^-}^{L_0^+} (d\mathbf{M}_{tot}) dx_{2D}
\end{aligned} \tag{3.32}$$

3.2.2 Additional Terms

Longitudinal Lift

Strip-theory is unsuitable for evaluating some terms, as one dimension should be large compared to the other. Following [36, 32, 76], C_{Z_β} is the lift coefficient dependent on angle of attack β :

$$\beta = \tan\left(\frac{w}{u}\right) \approx \frac{w}{u} \tag{3.33}$$

$$C_Z = \frac{-Z}{\frac{1}{2}\rho u^2 d^2} \tag{3.34}$$

$$C_{Z_\beta} = \frac{dC_Z}{d\beta} \tag{3.35}$$

for which Hoerner [32] defines $C_{Z_\beta} = 1.2 \text{rad}^{-1}$.

$$Z_w \approx -\frac{d}{dw} \left(\frac{1}{2} \rho u^2 W^2 C_{Z_\beta} \beta \right) = -\frac{1}{2} \rho u W^2 C_{Z_\beta} \tag{3.36}$$

$$Z_{uw} = \frac{Z_w}{u} = -\frac{1}{2} \rho W^2 C_{Z_\beta} \tag{3.37}$$

$$M_{uw} = -\frac{Z_w x_L}{u} = -\frac{1}{2} \rho W^2 C_{Z_\beta} x_L \tag{3.38}$$

where x_L is the vector from the center of lift to the body-fixed origin.

Thruster Guards and RTU

The drag F_{D_t} due to the thruster guards and RTU arms are modeled as follows:

$$X_{u|u|_t} = -\frac{1}{2}\rho C_d(A_{guards_x} + A_{RTU}) \quad (3.39)$$

$$Z_{w|w|_t} = -\frac{1}{2}\rho C_d(A_{guards_z} + A_{RTU}) \quad (3.40)$$

where $C_d=0.47$ is the drag coefficient for a sphere [31], A_{guards_x} and A_{guards_z} are the projected area of the thruster guard in the x - and z -directions, and A_{RTU} is the projected area of the RTU arms.

3.3 Hydrostatics

Following the methods in Fossen [24], the gravitational force \mathbf{f}_G acts at the center of mass, located a distance from the origin $\mathbf{r}_G = [x_G, y_G, z_G]^T$, and buoyant force \mathbf{f}_h acts at the center of buoyancy, located a distance from the origin $\mathbf{r}_h = [x_h, y_h, z_h]^T$. The vector of restoring forces and moments $\mathbf{g}(\boldsymbol{\eta})$ is

$$\mathbf{g}(\boldsymbol{\eta}) = - \begin{bmatrix} \mathbf{f}_G(\boldsymbol{\eta}) + \mathbf{f}_h(\boldsymbol{\eta}) \\ \mathbf{r}_G \times \mathbf{f}_G(\boldsymbol{\eta}) + \mathbf{r}_h \times \mathbf{f}_h(\boldsymbol{\eta}) \end{bmatrix} \quad (3.41)$$

Expanding these equations results in the nonlinear equations for hydrostatic forces and moments:

$$\begin{aligned} X_{HS} &= (W - B) \sin \theta \\ Y_{HS} &= -(W - B) \cos \theta \sin \phi \\ Z_{HS} &= -(W - B) \cos \theta \cos \phi \\ K_{HS} &= -(W y_G - B y_h) \cos \theta \cos \phi + (W z_G - B z_h) \cos \theta \sin \phi \\ M_{HS} &= (W z_G - B z_h) \sin \theta + (W x_G - B x_h) \cos \theta \cos \phi \\ N_{HS} &= -(W x_G - B x_h) \cos \theta \sin \phi - (W y_G - B y_h) \sin \theta \end{aligned} \quad (3.42)$$

3.4 Propulsion Model

In order to precisely control a marine vehicle, it is important to understand the dynamics of its propulsors. This is especially true for small vehicles moving at low speeds, where the vehicle dynamics can be dominated by the thruster. The fluid velocity incident on the propeller blade has two components: the axial velocity associated with vehicle motion, and the tangential velocity associated with the spinning of the propeller. The thrust developed is a function of the blade shape, the axial velocity, and the rotational speed.

Several additional factors complicate thruster dynamics for a hovering vehicle. In unsteady maneuvers, the flow into the thruster changes with time. This can lead to nonlinear thrust response which is dependent on the magnitude of command [83] and subject to deadband. Thrust may also exhibit forward/aft asymmetry due to blade shape, duct shape, and wake effects of the motor pod. Cross-flow components in the inflow can produce additional asymmetry, so that the net force produced does not act along the thruster axis.

The dynamics of an azimuthing thruster are further complicated by an additional controllable input: the azimuth angle, and its rate of change. A steady azimuth angle produces a cross-flow component to the inflow. A changing azimuth angle introduces another rotational component to the inflow, proportional to the azimuth rate, $\dot{\alpha}$ (rad/s).

The thrusters for the Odyssey IV AUV are speed-controlled, using pulse-width modulation (PWM) to control the propeller speed ω (rad/s), for which the equation for steady-state thrust T is as follows:

$$T = K_T \omega |\omega| \tag{3.43}$$

where K_T is a thruster constant equal to 0.0108 kg*m for the Odyssey IV thrusters. Since the focus of this thesis is hovering maneuvers without current disturbances, the thruster model for the vehicle is considered at zero-vehicle speed and in-flow and cross-flow velocities are considered negligible.

Experiments show that unsteady dynamics of an azimuthing thruster are quite complex. Preliminary analysis suggested that actual thrust produced has a time dependence and is affected by the rate of change of azimuth angle. For commanded thrust T_{des} , a simple model for the reduced thrust due to azimuthing $T_{\dot{\alpha}}$ at current azimuth rate $\dot{\alpha}$ was developed as follows:

$$T_{\dot{\alpha}} = \frac{T_{des}}{1 + k_{\dot{\alpha}} \frac{\dot{\alpha}}{\dot{\alpha}_{max}}} \quad (3.44)$$

where $\dot{\alpha}_{max}$ is the maximum azimuth rate and $k_{\dot{\alpha}}$ is an empirically determined coefficient. In addition, a time-dependent thrust model was developed. The reduced thrust $T_{\dot{\alpha}}$ is put through a first-order filter with gain λ_T , in order to simulate time-dependent thrust development:

$$\dot{T}_f = \lambda_T(T_{\dot{\alpha}} - T_f) \quad (3.45)$$

Figure 3-2 compares the thruster model with experimental results (the experiments are described in further detail in Section 4.3). The full thruster model with time- and azimuth rate-dependence improves performance of the full vehicle model. The vector $\boldsymbol{\tau}_{prop}$ represents the forces and moments on the vehicle from the propulsion system:

$$\boldsymbol{\tau}_{prop} = [X_{prop}, Y_{prop}, Z_{prop}, K_{prop}, M_{prop}, N_{prop}]^T \quad (3.46)$$

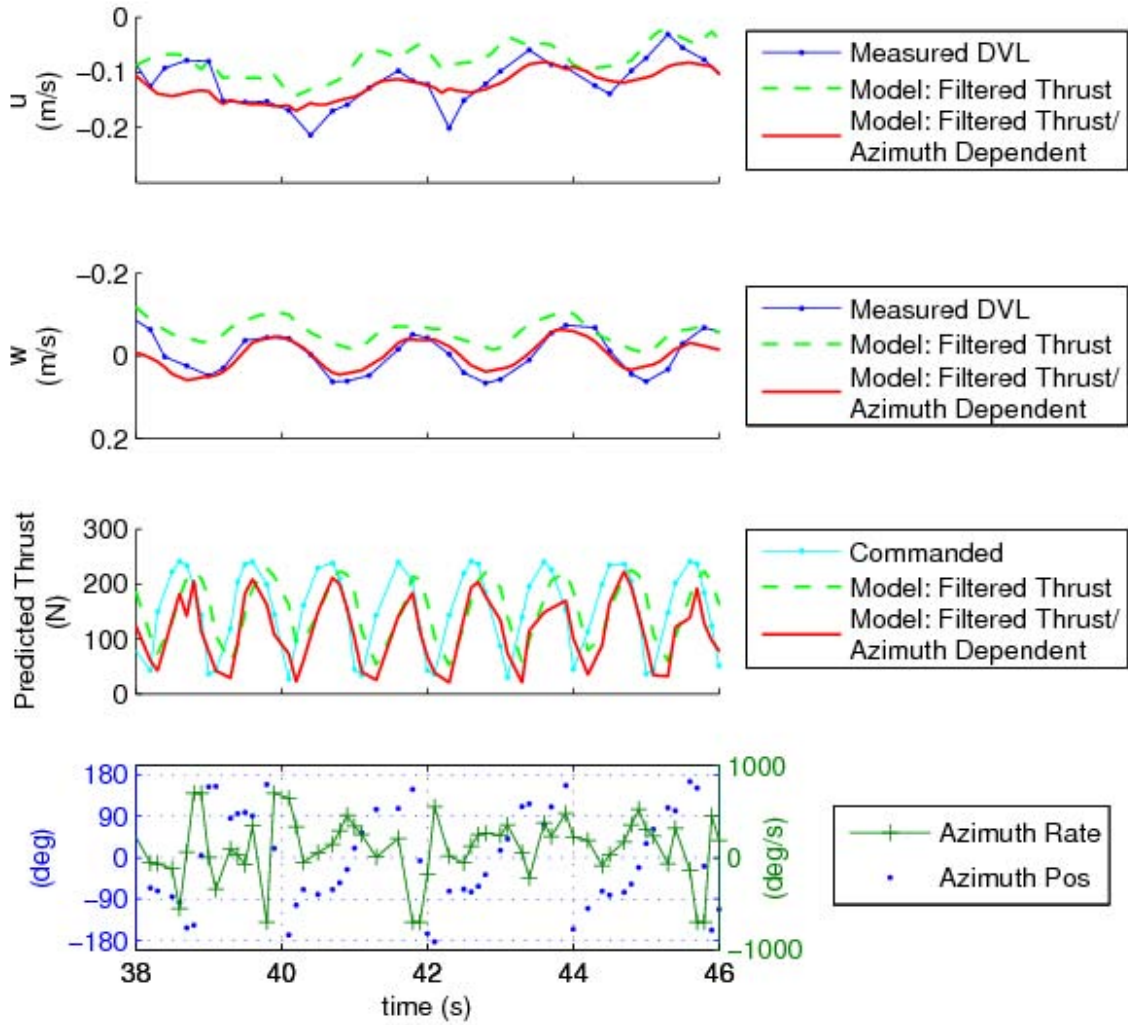


Figure 3-2: Unsteady Thrust Model: Comparison Between Measured and Predicted Vehicle Response. Thruster models include $\dot{T}_f = \lambda_T(T_{des} - T_f)$ which models time-dependence of thrust development, and $T_{\dot{\alpha}} = T_{des}/(1 + k_{\dot{\alpha}}\dot{\alpha}/\dot{\alpha}_{max})$ which models the azimuth rate dependence. Experiments suggest that the unsteady thrust development for an azimuthing propulsor is time dependent and reduced during azimuthing. Simulation constants: $\lambda_T = 7$, $k_{\dot{\alpha}} = 1$.

3.5 Complete Hydrodynamic Terms

Combining equations 3.6, 3.9 through 3.15, 3.32, 3.42, and 3.46, the sum of the forces and moments on the vehicle are expressed as:

$$\begin{aligned}
\sum X_{ext} &= X_{\dot{u}}\dot{u} + X_{u|u}|u| + X_{wq}wq + X_{q|q}|q| + X_{vr}vr + X_{r|r}|r| + \\
&\quad X_{HS} + X_{prop} \\
\sum Y_{ext} &= Y_{\dot{v}}\dot{v} + Y_{\dot{r}}\dot{r} + Y_{ur}ur + Y_{wp}wp + Y_{pq}pq + Y_{uv}uv + Y_{v|v}|v| + \\
&\quad Y_{r|r}|r| + Y_{HS} + Y_{prop} \\
\sum Z_{ext} &= Z_{\dot{w}}\dot{w} + Z_{\dot{q}}\dot{q} + Z_{uq}uq + Z_{vp}vp + Z_{rp}rp + Z_{uw}uw + Z_{w|w}|w| + \\
&\quad Z_{q|q}|q| + Z_{HS} + Z_{prop} \quad (3.47) \\
\sum K_{ext} &= K_{\dot{p}}\dot{p} + X_{p|p}|p| + K_{HS} + K_{prop} \\
\sum M_{ext} &= M_{\dot{w}}\dot{w} + M_{\dot{q}}\dot{q} + M_{uq}uq + M_{vp}vp + M_{rp}rp + M_{uw}uw + M_{w|w}|w| + \\
&\quad M_{q|q}|q| + M_{HS} + M_{prop} \\
\sum N_{ext} &= N_{\dot{v}}\dot{v} + N_{\dot{r}}\dot{r} + N_{ur}ur + N_{wp}wp + N_{pq}pq + N_{uv}uv + N_{v|v}|v| + \\
&\quad N_{r|r}|r| + N_{HS} + N_{prop}
\end{aligned} \tag{3.48}$$

Chapter 4

Complete Model and Testing

In this chapter, we develop the full nonlinear equations of motion, then build a simplified model based upon linearization and decoupling for use in simulations and controller design. Experimental response of the vehicle is used to to validate and refine the performance of the analytical model.

4.1 Combined Nonlinear Equations of Motion

The full nonlinear equations of motion are formed by combining the rigid body equations of motion (Equation 2.6) and the equations of external forces and moments on

the vehicle (Equation 3.47):

$$\begin{aligned}
m[\dot{u} + qw - rv + (\dot{q} + rp)z_G - (q^2 + r^2)x_G] &= X_{HS} + X_{prop} + X_{vr}vr + X_{r|r}r|r| + \\
&X_{\dot{u}}\dot{u} + X_{u|u}|u|u| + X_{wq}wq + X_{q|q}|q|q| \\
m[\dot{v} + ru - pw + (pq + \dot{r})x_G + (rq - \dot{p})z_G] &= Y_{HS} + Y_{prop} + Y_{ur}ur + Y_{wp}wp + \\
&Y_{pq}pq + Y_{uv}uv + Y_{v|v}|v|v| + Y_{r|r}r|r| + Y_{\dot{v}}\dot{v} + Y_{\dot{r}}\dot{r} \\
m[\dot{w} + pv - qu + (pr - \dot{q})x_G - (p^2 + q^2)z_G] &= Z_{HS} + Z_{prop} + Z_{uq}uq + Z_{vp}vp + \\
&Z_{rp}rp + Z_{uw}uw + Z_{w|w}|w|w| + Z_{q|q}|q|q| + Z_{\dot{w}}\dot{w} + Z_{\dot{q}}\dot{q} \tag{4.1} \\
I_x\dot{p} + I_{xz}r + (I_z - I_y)rq + I_{xz}pq - m[z_G(\dot{v} + ru - pw)] &= K_{HS} + K_{prop} + \\
&K_{\dot{p}}\dot{p} + X_{p|p}|p|p| \\
I_y\dot{q} + (I_x - I_z)pr + I_{xz}(r^2 - p^2) + m[z_G(\dot{u} + qw - rv) - x_G(\dot{w} + pv - qu)] &= \\
&M_{HS} + M_{prop} + M_{\dot{w}}\dot{w} + M_{\dot{q}}\dot{q} + M_{uq}uq + M_{vp}vp + M_{rp}rp + M_{uw}uw + \\
&M_{w|w}|w|w| + M_{q|q}|q|q| \\
I_z\dot{r} + I_{zx}p + (I_y - I_x)pq - I_{xz}qr + m[x_G(\dot{v} + ru - pw)] &= N_{HS} + N_{prop} + \\
&N_{\dot{v}}\dot{v} + N_{\dot{r}}\dot{r} + N_{ur}ur + N_{wp}wp + N_{pq}pq + N_{uv}uv + N_{v|v}|v|v| + N_{r|r}r|r|
\end{aligned}$$

Gathering the accelerations, the equations can be rewritten:

$$\begin{aligned}
(m - X_{\dot{u}})\dot{u} + mz_G\dot{q} &= m[-qw + rv - rpz_G + (q^2 + r^2)x_G] + \\
&\quad X_{u|u}|u|u| + X_{wq}wq + X_{q|q}|q|q| + X_{vr}vr + X_{r|r}|r|r| + X_{HS} + X_{prop} \\
(m - Y_{\dot{v}})\dot{v} + (mx_G - Y_{\dot{r}})\dot{r} - mz_G\dot{p} &= m[-ru + pw - pqx_G - rqz_G] + \\
&\quad Y_{ur}ur + Y_{wp}wp + Y_{pq}pq + Y_{uv}uv + Y_{v|v}|v|v| + Y_{r|r}|r|r| + Y_{HS} + Y_{prop} \\
(m - Z_{\dot{w}})\dot{w} - (Z_{\dot{q}} + mx_G)\dot{q} &= m[-pv + qu - prx_G + (p^2 + q^2)z_G] + Z_{uq}uq + \\
&\quad Z_{vp}vp + Z_{rp}rp + Z_{uw}uw + Z_{w|w}|w|w| + Z_{q|q}|q|q| + Z_{HS} + Z_{prop} \\
(I_x - K_{\dot{p}})\dot{p} - mz_G\dot{v} &= -I_{xz}r - (I_z - I_y)rq - I_{xz}pq + m[z_G(ru - pw)] \\
&\quad + X_{p|p}|p|p| + K_{HS} + K_{prop} \\
(I_y - M_{\dot{q}})\dot{q} - (mx_G + M_{\dot{w}})\dot{w} + mz_G\dot{u} &= (-I_x + I_z)pr - I_{xz}(r^2 - p^2) - \\
&\quad m[z_G(qw - rv) - x_G(pv - qu)] + M_{uq}uq + M_{vp}vp + M_{rp}rp + \\
&\quad M_{uw}uw + M_{w|w}|w|w| + M_{q|q}|q|q| + M_{HS} + M_{prop} \\
(I_z - N_{\dot{r}})\dot{r} + (mx_G - N_{\dot{v}})\dot{v} &= -I_{zx}p - (I_y - I_x)pq + I_{xz}qr - m[x_G(ru - pw)] \\
&\quad + N_{ur}ur + N_{wp}wp + N_{pq}pq + N_{uv}uv + N_{v|v}|v|v| + N_{r|r}|r|r| + N_{HS} + N_{prop}
\end{aligned} \tag{4.2}$$

These equations can then be written in the matrix form of Newton's second law as follows, such that $\mathbf{A}\dot{\boldsymbol{\nu}} = \sum \mathbf{F}$:

$$\begin{bmatrix}
m - X_{\dot{u}} & 0 & 0 & 0 & mz_g & 0 \\
0 & m - Y_{\dot{v}} & 0 & -mz_G & 0 & mx_G - Y_{\dot{r}} \\
0 & 0 & m - Z_{\dot{w}} & 0 & -mx_G - Z_{\dot{q}} & 0 \\
0 & -mz_G & 0 & I_x - K_{\dot{p}} & 0 & 0 \\
mz_G & 0 & -mx_G - M_{\dot{w}} & 0 & I_y - M_{\dot{q}} & 0 \\
0 & mx_G - N_{\dot{v}} & 0 & 0 & 0 & I_z - N_{\dot{r}}
\end{bmatrix}
\begin{bmatrix}
\dot{u} \\
\dot{v} \\
\dot{w} \\
\dot{p} \\
\dot{q} \\
\dot{r}
\end{bmatrix}
=
\begin{bmatrix}
\sum X \\
\sum Y \\
\sum Z \\
\sum K \\
\sum M \\
\sum N
\end{bmatrix} \tag{4.3}$$

4.2 Simplified Model

4.2.1 Linearized Equations of Motion

The equations of motion are linearized to make the control problem more tractable, such that the nonlinear state equation

$$\dot{\mathbf{x}} = \mathbf{f}(\mathbf{x}, \mathbf{u}) \quad (4.4)$$

is transformed into the form

$$\mathbf{A}_0 \dot{\mathbf{x}} = \mathbf{B}_0 \mathbf{x} + \boldsymbol{\tau}_{prop} \quad (4.5)$$

where \mathbf{A}_0 and \mathbf{B}_0 are the matrices associated with the linearized equations of motion, while the vector $\boldsymbol{\tau}_{prop}$ represents the forces and moments on the vehicle due to the propulsion system.

The linearized equations of motion are formulated by linearizing about time-varying reference trajectories $\boldsymbol{\nu}_0(t)$ and $\boldsymbol{\eta}_0(t)$:

$$\boldsymbol{\nu}_0 = [u_0, v_0, w_0, p_0, q_0, r_0]^T; \quad \boldsymbol{\eta}_0 = [x_0, y_0, z_0, \phi_0, \theta_0, \psi_0]^T \quad (4.6)$$

where perturbations are described as the following differentials:

$$\Delta \boldsymbol{\nu} = \boldsymbol{\nu} - \boldsymbol{\nu}_0; \quad \Delta \boldsymbol{\eta} = \boldsymbol{\eta} - \boldsymbol{\eta}_0; \quad (4.7)$$

Following Fossen [24], we use the vector notation:

$$\mathbf{f}_c(\boldsymbol{\nu}) = \mathbf{C}(\boldsymbol{\nu})\boldsymbol{\nu}; \quad \mathbf{f}_d(\boldsymbol{\nu}) = \mathbf{D}(\boldsymbol{\nu})\boldsymbol{\nu}; \quad (4.8)$$

Neglecting 2nd-order terms, 2.15 and 2.16 can be linearized as follows:

$$\mathbf{M} \Delta \dot{\boldsymbol{\nu}} + \left. \frac{\partial \mathbf{f}_c(\boldsymbol{\nu})}{\partial \boldsymbol{\nu}} \right|_{\boldsymbol{\nu}_0} \Delta \boldsymbol{\nu} + \left. \frac{\partial \mathbf{f}_d(\boldsymbol{\nu})}{\partial \boldsymbol{\nu}} \right|_{\boldsymbol{\nu}_0} \Delta \boldsymbol{\nu} + \left. \frac{\partial \mathbf{g}(\boldsymbol{\eta})}{\partial \boldsymbol{\eta}} \right|_{\boldsymbol{\eta}_0} \Delta \boldsymbol{\eta} \quad (4.9)$$

$$\dot{\boldsymbol{\eta}}_0 + \Delta \dot{\boldsymbol{\eta}} \approx \mathbf{J}(\boldsymbol{\eta}_0 + \Delta \boldsymbol{\eta}) + \frac{\partial \mathbf{J}(\boldsymbol{\eta}) \boldsymbol{\nu}}{\partial \boldsymbol{\eta}} \Big|_{\boldsymbol{\nu}_0, \boldsymbol{\eta}_0} \Delta \boldsymbol{\nu} + \frac{\partial \mathbf{J}(\boldsymbol{\eta}) \boldsymbol{\nu}}{\partial \boldsymbol{\nu}} \Big|_{\boldsymbol{\nu}_0, \boldsymbol{\eta}_0} \Delta \boldsymbol{\eta}. \quad (4.10)$$

This reduces to

$$\Delta \dot{\boldsymbol{\eta}} \approx \mathbf{J}(\boldsymbol{\eta}_0) \Delta \boldsymbol{\nu} + \frac{\partial \mathbf{J}(\boldsymbol{\eta})}{\partial \boldsymbol{\eta}} \Big|_{\boldsymbol{\eta}_0} \boldsymbol{\nu}_0 \Delta \boldsymbol{\eta} \quad (4.11)$$

We define a new state vector $\mathbf{x} = (\Delta \boldsymbol{\nu}, \Delta \boldsymbol{\eta})^T$. A new formulation, with linearized equations of motion and nonlinear control input vector is now

$$\dot{\mathbf{x}} = \begin{bmatrix} -\mathbf{M}^{-1}(\mathbf{C} + \mathbf{D}) & -\mathbf{M}^{-1}\mathbf{G} \\ \mathbf{J} & \partial \mathbf{J}(\boldsymbol{\eta}) / \partial \boldsymbol{\eta} \end{bmatrix} \mathbf{x} + \begin{bmatrix} -\mathbf{M}^{-1} \\ 0 \end{bmatrix} \boldsymbol{\tau}_{prop} \quad (4.12)$$

The coefficients for $-\mathbf{M}^{-1}(\mathbf{C} + \mathbf{D})$ can be found in Appendix B.

4.2.2 Decoupled Linear Model

The dynamic model of the Odyssey IV AUV is described in Chapter 2. Since the focus of this thesis is maneuvering with the rotating thruster unit, meaning, motion in the surge, heave and pitch directions, we are interested in reducing the number of states for ease in computation. Healey [28] suggests that the AUV model can be separated into subsystems due to negligible interactions between the states for certain behaviors. From this work, it is suggested that the forward (u, x) and diving (w, q, θ, z) directions can be decoupled from the remaining states (v, p, r, ϕ, ψ). We therefore are interested in the following states of the vehicle model: $[u, w, x, z, q, \theta]$. See Appendix B for the model coefficient matrices.

4.3 Validation/Adjustment

4.3.1 Testing Description

Experimental results are required to determine the accuracy of the model. Tests were performed in the engineering tank at the Jere A. Chase Ocean Engineering Laboratory at the University of New Hampshire (UNH), which measures 60 x 40 x 20 feet. The vehicle's response was measured using the sensors described in Table 2.1. Vehicle

position when submerged was estimated using integration of the raw DVL velocities and/or an Extended Kalman Filter.

4.3.2 Figures and Analysis

All tests were performed at depth and at near-zero starting speed, such that surface effects can be ignored. Figure 4-1 demonstrates the vehicle response to step changes in thrust direction at constant thrust command. Figure 4-2 compares the actual vehicle response to the prediction model. As can be seen, the original model was slightly underdamped in heave and surge, so hydrodynamic coefficients for the model are adjusted accordingly in figure 4-2.

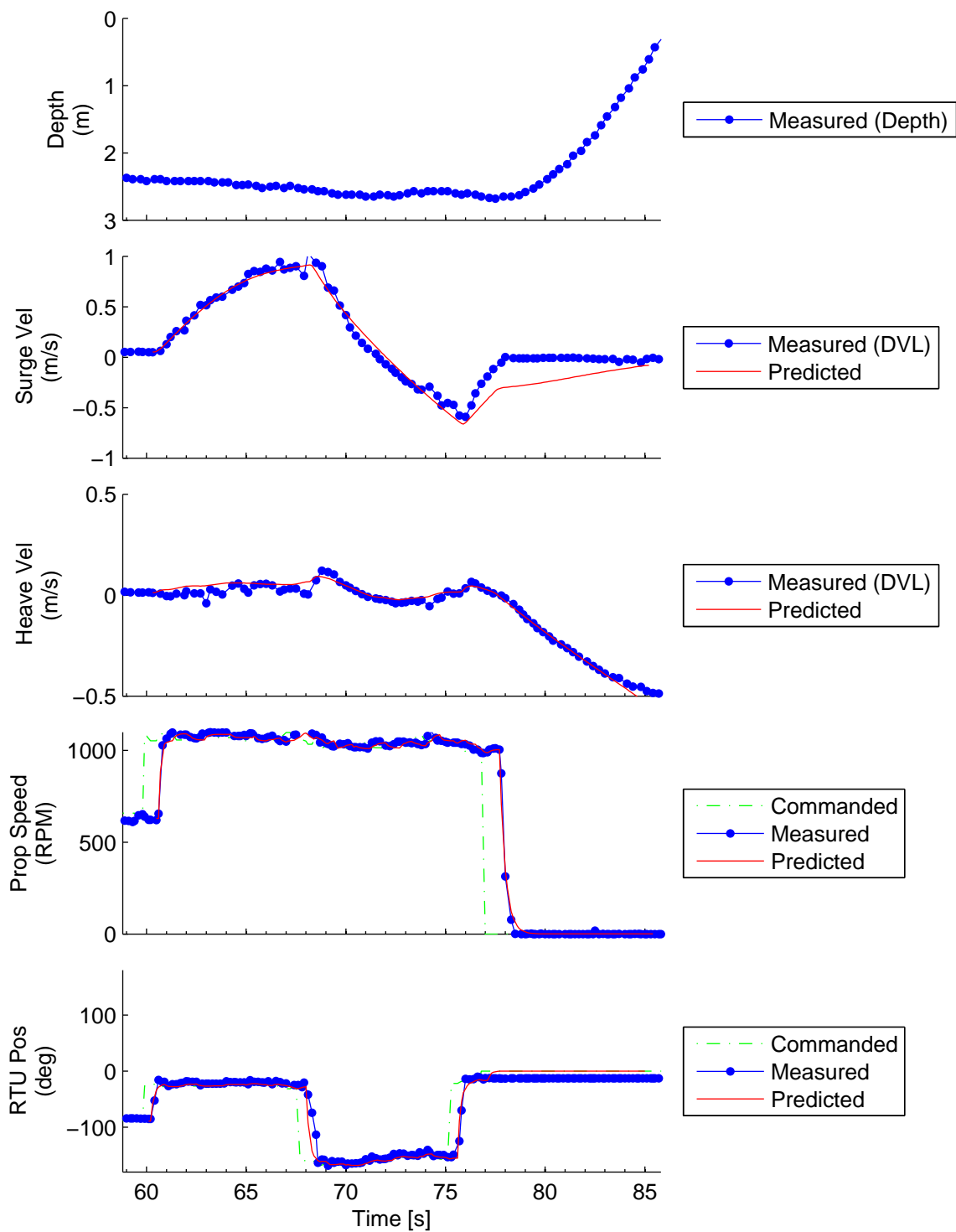


Figure 4-1: Experimental vehicle response to forcing in surge. The vehicle was brought to depth such that surface effects could be ignored in analysis. Thrust commands were alternated between forcing in positive surge and forcing in negative surge, with each command held constant for 8 seconds.

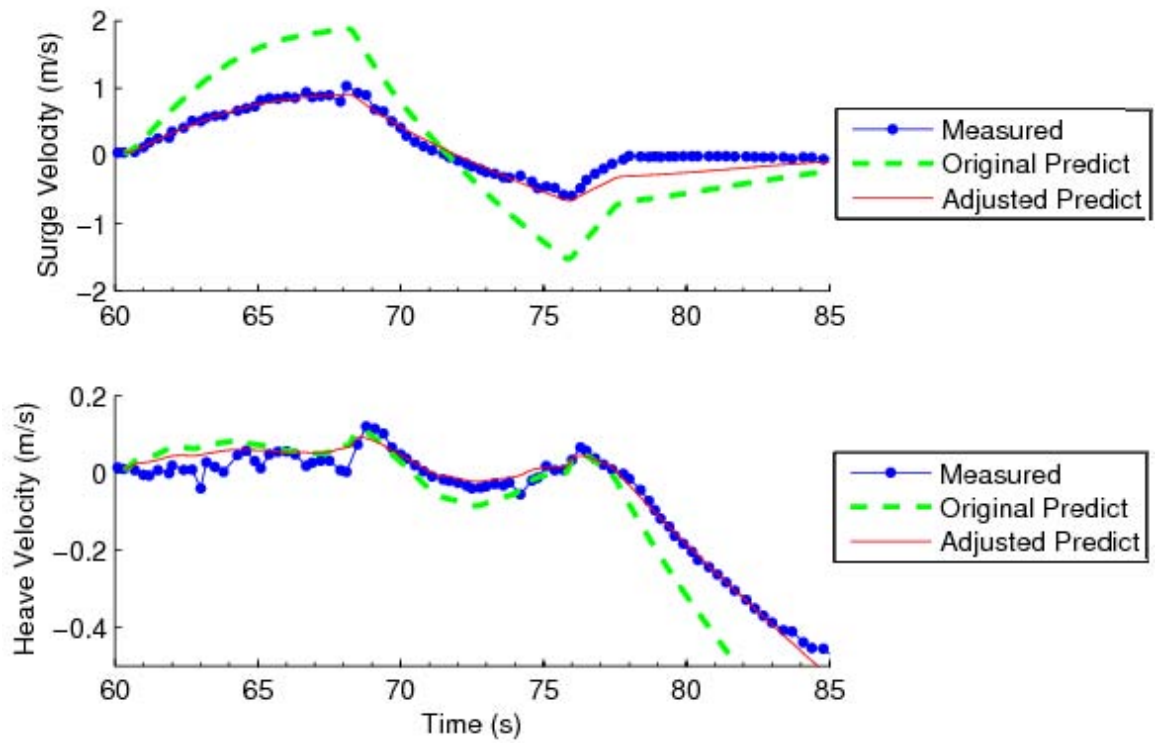


Figure 4-2: Comparison between measured and predicted vehicle response to forcing in surge. The prediction model is given the control inputs from the experiment seen in figure 4-1, and the original vehicle/propulsion model is shown to have similar behavior. Hydrodynamic coefficients are adjusted to achieve better model performance

Chapter 5

Controller Design

Control design for the Odyssey IV AUV requires using the azimuthing thruster to control position in both the surge and heave directions. The goal of this work is to develop a controller that allows the vehicle to perform maneuvers in a minimum-time manner that handles the physical constraints in the propulsion system. The cross-body thrusters are not considered in this analysis. In this chapter, the current controller for the Odyssey IV is considered, and a nonlinear control scheme is introduced.

5.1 Algorithm Description

5.1.1 PID

Proportional-integral-derivative (PID) control is widely used in industry and is a well understood technique [60, 61]. PID works on the principle of closed-loop feedback, where the proportional term P is linear to error, integral term I goes with the accumulation of error over time, and the derivative term D goes with the derivative of the error. Defining controller output $u(t)$, the closed-loop control law is of the form:

$$u(t) = k_p e(t) + k_i \int_0^t e(\tau) d\tau + k_d \frac{de}{dt} \quad (5.1)$$

where k_p is the proportional gain, k_i is the integral gain, and k_d is the derivative gain. Gains can be tuned according to the desired response with the tradeoffs inherent. Proportional control can increase the system responsiveness, however, if k_p is too large it can drive the system to instability. Increasing derivative gain k_d increases damping and reduces overshoot, but can lead to steady-state error. Adding integral control k_i reduces steady-state error, however, it can cause overshoot. Careful tuning is required to achieve fast response and stability. The existing closed-loop control for

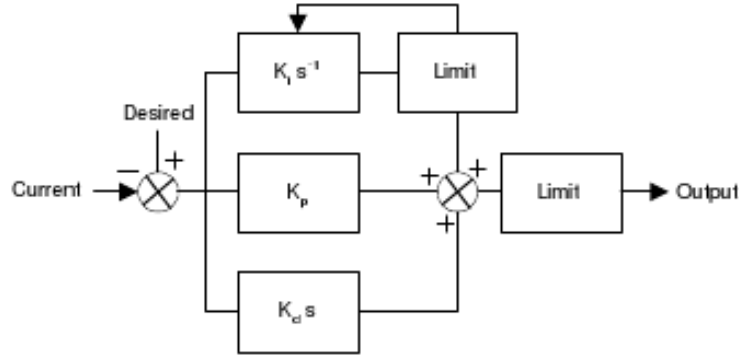


Figure 5-1: Structure of MOOS PID (image source:[59])

the Odyssey IV consists of PID (see figure 5-1), in concert with internal thrust and RTU controllers. Appropriate PID gains were empirically determined. The control law for each axis (heave, surge) is solved using position errors to find the desired control action for that axis, namely the desired forces in heave F_{heave} and surge F_{surge} . The control inputs to the rotating thruster unit are thrust u_T and azimuth angle u_α , found from a mapping of the control actions from Cartesian to polar coordinates as follows:

$$u_T = \sqrt{F_{heave}^2 + F_{surge}^2} \quad (5.2)$$

$$u_\alpha = \arctan\left(\frac{F_{heave}}{F_{surge}}\right) \quad (5.3)$$

PID has huge advantages in that it has been widely applied in industry and analysis is detailed. Although PID is a linear controller, it has been successfully applied to many nonlinear systems. Performance can certainly degrade if operating outside of

the linearized regime. In addition, the PID controller has no knowledge of the system itself.

Closed-Loop PID Experimental Performance

Figure 5-2 demonstrates the performance of the existing PID controller for the Odyssey IV, maneuvering to waypoints in surge at depth. Figure 5-3 shows the data from Fig-

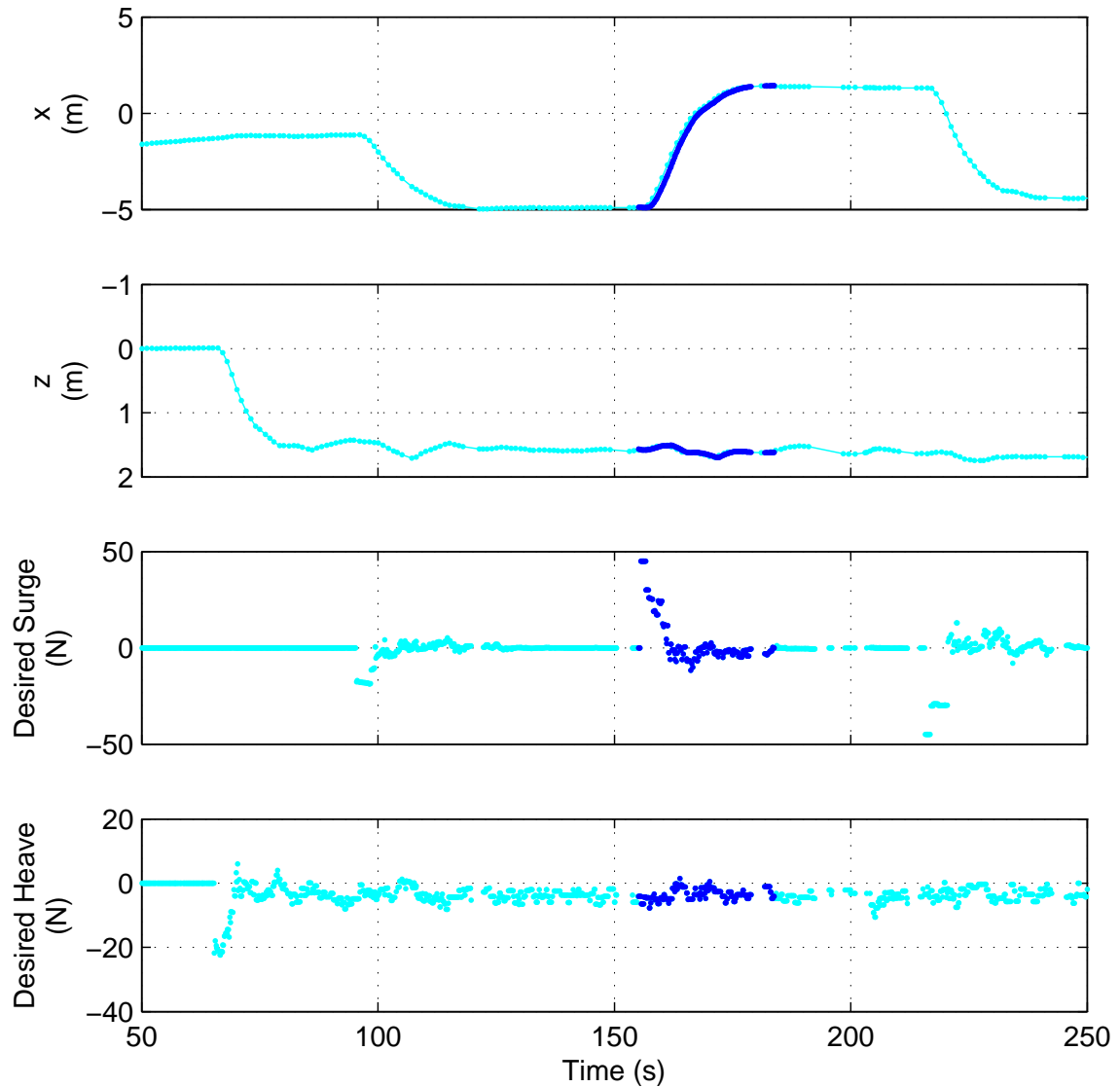


Figure 5-2: Closed-loop PID response: Response to step change in desired surge position (+6m) at depth, for slightly positively buoyant vehicle. The highlighted time range [155s 184s] is used to illustrate the commanded thrust vectors at each position, seen in figure 5-3

ure 5-2 from the highlighted time range [155s 184s]. The desired thrust vector at each position is shown, with desired waypoint approximately 1.4m forward in surge. Note that because the vehicle buoyancy is slightly positive, some amount of desired forcing in the negative heave direction is required in addition to the force required for the surge maneuver. It is seen that in these experiments the PID controller commands

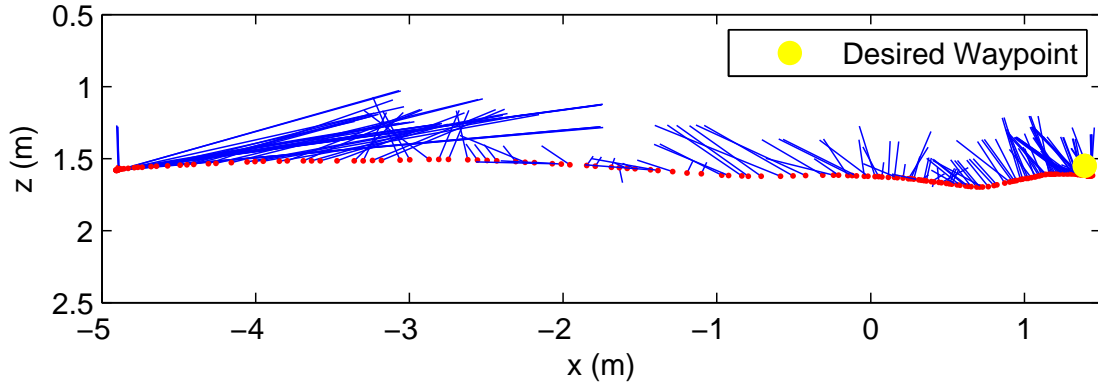


Figure 5-3: Closed-loop PID response: Commanded thrust vectors for response to step change in desired surge position (+6m) at depth, for slightly positively buoyant vehicle. The full vehicle response is shown in figure 5-2

fairly cautious control actions. The gains could be tuned for more aggressive maneuvers, but since there is no knowledge of the system, control could be compromised. For operations requiring complex maneuvers, a more advanced controller becomes necessary.

5.1.2 Model Predictive Controller

Model predictive control (MPC) is an attractive solution to the azimuthing thruster problem, as it leverages knowledge of the system, allows the inclusion of constraints within the formulation of the optimization problem, and solves an optimal control law based upon the current state of the plant. MPC solves for a control action by minimizing a performance objective function over a finite prediction time horizon T_p . The controller predicts the system response based upon a projection forward integration of a system model, solving for the required control action in order to achieve the desired response over the time horizon. In an ideal world where there were

no modeling errors, no disturbances, and computational time was not an issue, the optimization problem could be solved over an infinite time horizon and the control action could be played through eternity. Since the world is not ideal, feedback is required to correct errors. MPC formulates the problem over a finite prediction time horizon, and plays back the control action until the next sampling time. Then, the objective function is reformulated using the current plant state as the initial state, and the process is repeated. The focus of this work is formulating a quadratic cost function based on vehicle states. Other cost function choices can be found in sources such as [44].

Linear MPC

Linear MPC, in which a linear model of the system dynamics is used for prediction, is a well-established method of control and has a range of applications in industry [26, 66]. Linear MPC theory is extensive, with regards to design and performance characteristics such as computational speed, stability, and robustness [46, 54]. The linear discrete time model is of the form:

$$x(k+1) = Ax(k) + Bu(k) \tag{5.4}$$

$$y(k) = Cx(k) \tag{5.5}$$

where x_k and u_k represent the state and control input at discrete time event k . By using this state-space form, linear systems theory is applicable. The on-line solution of the optimization problem is relatively simple, and closed-loop analysis is well-understood.

Many systems have physical constraints on states and inputs. Therefore, it is desirable to incorporate these constraints into the MPC problem. However, the addition

of constraints to the linear model adds a level of complexity:

$$x(k+1) = Ax(k) + Bu(k) \quad (5.6)$$

$$y(k) = Cx(k) \quad (5.7)$$

$$Du(k) \leq d \quad (5.8)$$

$$Hx(k) \leq h \quad (5.9)$$

where D and H represent the constraint matrices, and d and h are positive vectors. The constrained optimal control problem is understood, however, the problem of solving the constrained optimal control problem for a moving horizon becomes more difficult [68].

Nonlinear MPC

The application of MPC to nonlinear systems has gained much interest in the past 20 years. Many systems are inherently nonlinear, and in some cases, a linear model is not adequate because operations may be outside of the linear regime. In these cases, there are advantages to prediction using a nonlinear model. There are a number of good reviews regarding nonlinear MPC techniques, including [6, 22, 30, 46].

We formulate the discrete-time system

$$x(k+1) = f(x(k), u(k)) \quad (5.10)$$

$$y(k) = g(x(k)) \quad (5.11)$$

where f is a nonlinear function of state $x(k)$ and control input $u(k)$ for discrete time event k . Letting positive integer N denote the prediction horizon, we define discrete state sequence \mathbf{x} such that $\mathbf{x} = x(0), x(1), \dots, x(N)$ and discrete control input sequence \mathbf{u} such that $\mathbf{u} = u(0), u(1), \dots, u(N-1)$. We now define the objective function $J_N(\mathbf{x}, \mathbf{u})$ for prediction horizon N to be

$$\min_{\mathbf{x}, \mathbf{u}} J_N(\mathbf{x}, \mathbf{u}) \quad \text{subject to } u_L \leq \mathbf{u} \leq u_U \quad (5.12)$$

where u_L and u_U are the upper and lower bounds on the control input \mathbf{u} .

Theory and Application The theory and application of nonlinear MPC is far less developed compared to that of linear MPC. One large area of research involves improving the reliability and reducing the computational cost of the on-line optimization problem [7, 11, 21], which is much more complex than that of the convex quadratic problem of linear MPC. System theory topics such as robust stabilization are also highly of interest [11, 17, 67], however, the majority of the work is useful in theory and understanding, and current solutions are not transferable to practice.

Nonlinear MPC has been used in a limited range of applications in industry [65]. These applications largely depend on slow dynamics relative to the time required to perform the optimization [8]. Stability constraints are generally not considered from a feasibility of practice standpoint.

Chapter 6

Nonlinear Constrained Model Predictive Controller

In this chapter we investigate the use of nonlinear model predictive control for the Odyssey IV AUV. The performance optimization function is formulated from the prediction model developed in previous chapters. Optimization routines are described and their performance is evaluated. A nonlinear model predictive controller simulation is developed. Several experimental controller variations are considered, and compared to the simulation results.

6.1 Introduction

Nonlinear constrained model predictive control requires the on-line solution of an open-loop optimal control problem. A nonlinear model is used for prediction and constraints are enforced within the formulation of the performance optimization function. Feedback consists of applying the control action between sampling instances until the optimization problem can be re-formulated and re-solved using the current measured states.

6.1.1 Problem Formulation

In order to include the propulsion model within the state equations (refer to Section 3.4 for the description of the propulsion model), we include thrust T and azimuth angle α within new state vector \mathbf{x} , and control input vector \mathbf{u} comprised of commanded control inputs defined as commanded thrust u_T and commanded azimuth rate $u_{\dot{\alpha}}$:

$$\mathbf{x} = (u, w, x, z, q, \theta, T, \alpha)^T \quad (6.1)$$

$$\mathbf{u} = [u_T, u_{\dot{\alpha}}]^T \quad (6.2)$$

with the equations of motion for the vehicle dynamic model linearized about time-varying reference trajectories while still maintaining the nonlinearities in commanded control inputs as discussed in Section 4.2.1:

$$\dot{\mathbf{x}} = f(\mathbf{x}, \mathbf{u}), \quad \mathbf{x}(0) = \mathbf{x}_0. \quad (6.3)$$

In order to distinguish between actual and prediction, predicted states and inputs used in the optimization will be denoted as \hat{x} and \hat{u} . Because we are concerned with performing maneuvers in the surge and heave directions, the cost function will be formulated of the following predicted state vector $\hat{\mathbf{x}}(k)$ for discrete time instance k

$$\hat{\mathbf{x}}(k) = [\hat{u}(k), \hat{w}(k), \hat{x}(k), \hat{z}(k)]^T \quad (6.4)$$

The predicted states are found using a forward integration of the model using a fourth-order runge-kutta method [63] for initial conditions obtained at the start of optimization.

Referring to 5.12, the discrete cost function J specifying the desired control performance is defined as follows, for the vector of control actions $\hat{\mathbf{u}}$ used to simulate the

system:

$$\min_{\hat{\mathbf{u}}} J = \sum_{k=0}^N \hat{\mathbf{x}}(k)^T \mathbf{Q} \hat{\mathbf{x}}(k) \quad (6.5)$$

$$\text{subject to } u_{T,\min} \leq \hat{\mathbf{u}}_T \leq u_{T,\max} \quad (6.6)$$

$$u_{\dot{\alpha},\min} \leq \hat{\mathbf{u}}_{\dot{\alpha}} \leq u_{\dot{\alpha},\max} \quad (6.7)$$

where Q is the weighting matrix. The solution of 6.5 is found to be

$$\hat{\mathbf{u}}_T^* = [\hat{u}_T^*(0), \hat{u}_T^*(1), \dots, \hat{u}_T^*(N-1)]^T \quad (6.8)$$

$$\hat{\mathbf{u}}_{\dot{\alpha}}^* = [\hat{u}_{\dot{\alpha}}^*(0), \hat{u}_{\dot{\alpha}}^*(1), \dots, \hat{u}_{\dot{\alpha}}^*(N-1)]^T \quad (6.9)$$

In a closed-loop form, the first element $[\hat{u}_T^*(0), \hat{u}_{\dot{\alpha}}^*(0)]$ would be applied, the optimization problem would be reformed using the current states and solved again.

6.2 Optimization Methods

The implementation of nonlinear MPC on the Odyssey IV requires the real-time solution of a nonlinear, bound-constrained, optimal control problem. Following [22], the performance optimization problem is formulated as follows. The state sequence $\hat{\mathbf{x}}$ is described to lie in the connected, convex set of feasible states \mathbb{X} , and control sequence $\hat{\mathbf{u}}$ in the compact, convex set of feasible inputs \mathbb{U} . Cost function J is assumed to be a convex function. For relation $\dot{\mathbf{x}}(t) = \mathbf{f}(\mathbf{x}(t), \mathbf{u}(t))$, the nonlinear function \mathbf{f} is continuous.

As the vehicle model was developed using MATLAB, the search for an optimization routine began with pre-existing MATLAB functions. Several “off-the-shelf” methods that could be used efficiently within the MOOS architecture (C++) were also investigated. Performance characteristics of interest included: calculation time, robustness to range of initial states, and handling of bound constraints. Descriptions of the primary routines investigated follow, and performance comparisons for these can be seen in Section 6.2.2.

6.2.1 Methods

fminsearch

The MATLAB *fminsearch* function uses a Nelder-Mead or downhill simplex method [38]. A simplex is defined as an n -dimensional polytope created from a set of $n + 1$ points—a 1-simplex results in a line, a 2-simplex results in a triangle, a 3-simplex results in a tetrahedron, etc. This method involves creating a simplex from the values of the objective function. At each iteration, the algorithm generates a new point near the current simplex, and compares the function value with the current vertices of the simplex. If this new point results in a better function value than the current simplex, then we replace the vertex that results in the worst function value with the current point, creating a new simplex. This continues until the size of the simplex meets the specified tolerance.

Because *fminsearch* does not account for constraints within the problem formulation, *fminsearchbnd*, a peer-reviewed function from the MATLAB C File Exchange (see [15] for more details) has been developed to transform a simple bound-constrained optimization problem into an unconstrained problem that can be used with *fminsearch*.

lsqnonlin

The MATLAB nonlinear least-squares solver *lsqnonlin* uses a trust-region method [75, 12], which the documentation defines as finding a simpler quadratic approximation (using the first two terms of a Taylor approximation) to the objective function in the operating neighborhood, or “trust-region”. A two-dimensional subspace is formulated and solved using a preconditioned conjugate gradient approach. The size of the trust-region is adjusted until the desired convergence is achieved.

OptFDNIPS

Interior-point algorithms have shown promising results in nonlinear MPC [8, 81, 82]. *OPT++* [48] is a C++ class library for nonlinear optimization. The library includes

OptFDNIPS, an algorithm that uses a nonlinear interior-point method to solve bound-constrained nonlinear optimization problems. It can use line search or trust-region approaches. The merit function used in this work is a primal-dual path-following method, meaning it approximates a central path by taking Newton steps.

6.2.2 Performance

Computation time and robustness are compared for each of the methods discussed in Section 6.2.1. Different initial states of the optimization problem and initial control action guesses are used. The solution and resulting prediction model performance for one condition is shown in figure 6-1, and the computational time for each is listed in Table 6.1. The *OptFDNIPS* is clearly the fastest solver. Although it was not

Table 6.1: Optimization performance comparison for solving MPC open-loop problem

Algorithm	Calculation Time (s)
<i>lsqnonlin</i>	962
<i>OptFDNIPS</i>	0.2
<i>fminsearchbnd</i>	81

considered fast enough for the purposes of an on-line optimization solution, *OptFDNIPS* is still a promising result. For the purposes of performing off-line optimization solutions, however, *lsqnonlin* was found to be more robust in terms of initial starting conditions for the optimization routine.

6.3 Controller Simulation and Experimental Results

Vehicle controller tests were performed in the UNH engineering tank described in Section 4.3.1. Because a method for on-line calculation of the MPC optimization problem was not developed in time for this thesis, all experiments for the MPC controller use a pre-computed optimization solution using the MATLAB *lsqnonlin* function described above in Section 6.2.1. As was noted previously, all tests were

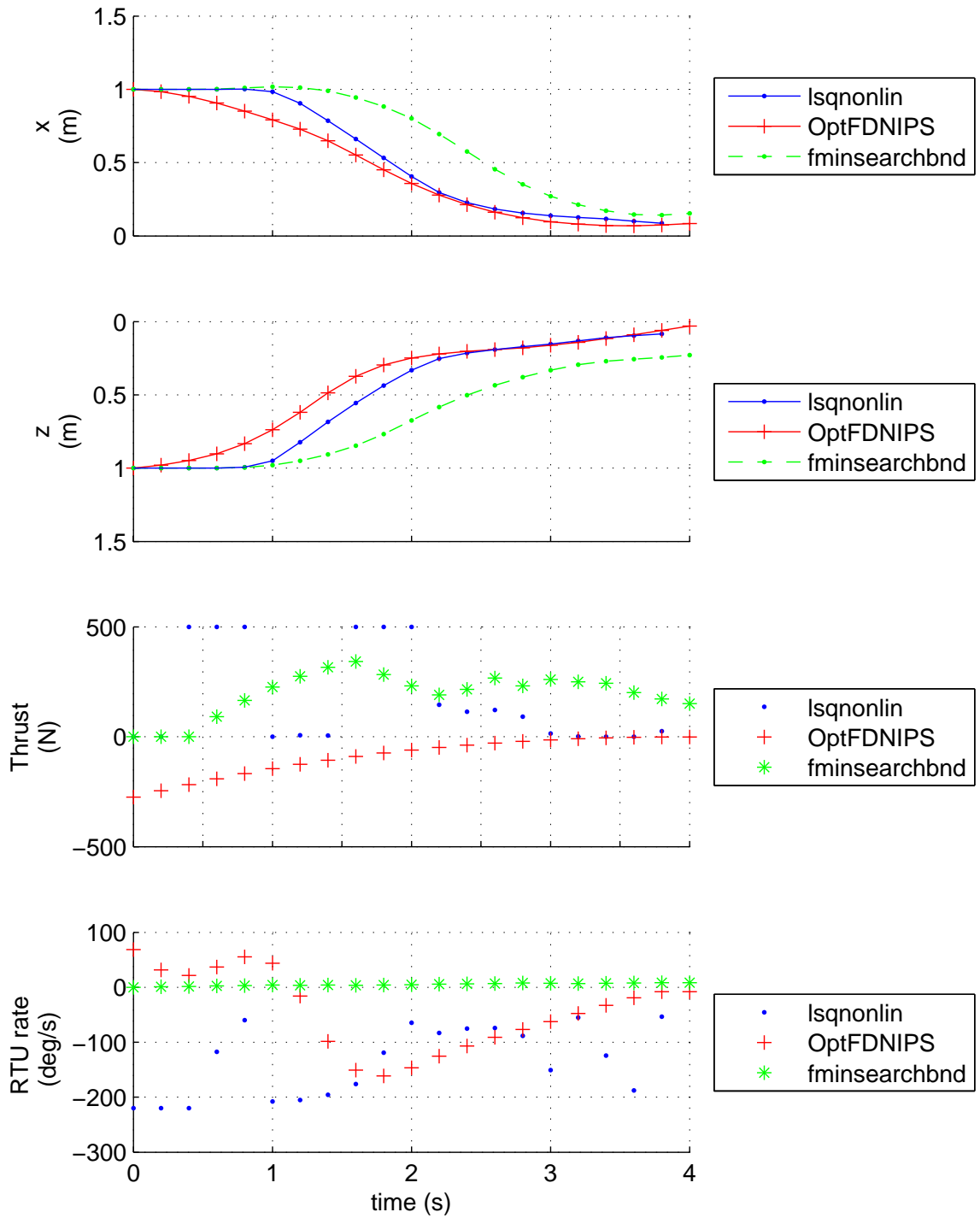


Figure 6-1: Performance comparison between optimization methods: Solving MPC open-loop problem for step change in desired surge position (+1m) and heave position (+1m). The computational time for each algorithm is listed in Table 6.1. MPC characteristics: $N=20$, $\Delta t=0.2s$. Bound conditions: $u_T=[0(N), 500(N)]$, $u_{\dot{\alpha}}=[-220(deg/s) 220(deg/s)]$

performed at depth and at near-zero starting speed, such that surface effects can be ignored.

6.3.1 PID Closed-Loop Simulation vs PID Closed-Loop Experiment

A PID simulation using the prediction model was developed for comparison to the existing PID controller for the Odyssey IV. The responses of the simulated PID controller and the actual are shown in figure 6-2. It is seen that the proportional gain k_P is equivalent. However, the model has less damping than the actual vehicle as k_D must be increased.

6.3.2 MPC Open-Loop Simulation vs PID Closed-Loop Experiment

The advantage of MPC over a traditional controller, such as the existing PID closed-loop controller, is that it builds upon a prediction model and directly enforces constraints. Figure 6-3 demonstrates the improvement in performance that an MPC controller could have over a traditional PID. Because the MPC has future knowledge of the system behavior, it is able to perform more aggressive maneuvers. In both the surge and heave positions, the MPC controller settles approximately 20s faster than the PID controller.

6.3.3 MPC Open-Loop Simulation vs MPC Open-Loop Experiment

This section represents the first step towards the implementation of MPC on an actual vehicle. An open-loop MPC controller was developed for the Odyssey IV AUV. The MPC optimization problem was calculated off-line using the MATLAB *lsqnonlin* function, and the appropriate solution for each time step was sent to the MOOS control. Figure 6-4 demonstrates the performance of this experimental open-loop MPC

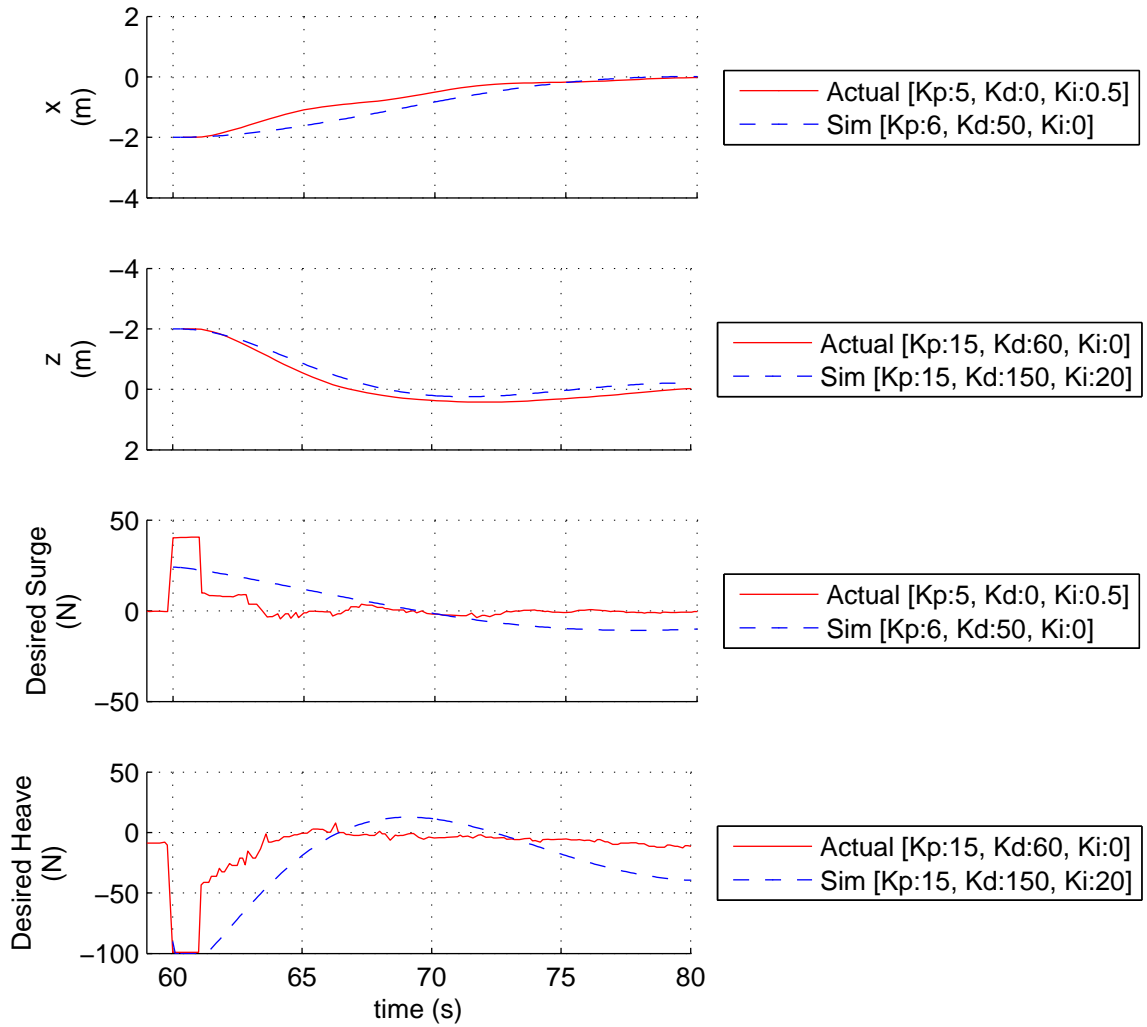


Figure 6-2: Comparison between closed-loop PID simulation and experiment: Response to step change in desired surge and heave position. The model has the appropriate stiffness, but less damping than the actual vehicle, judging by the PID coefficients required to achieve similar response

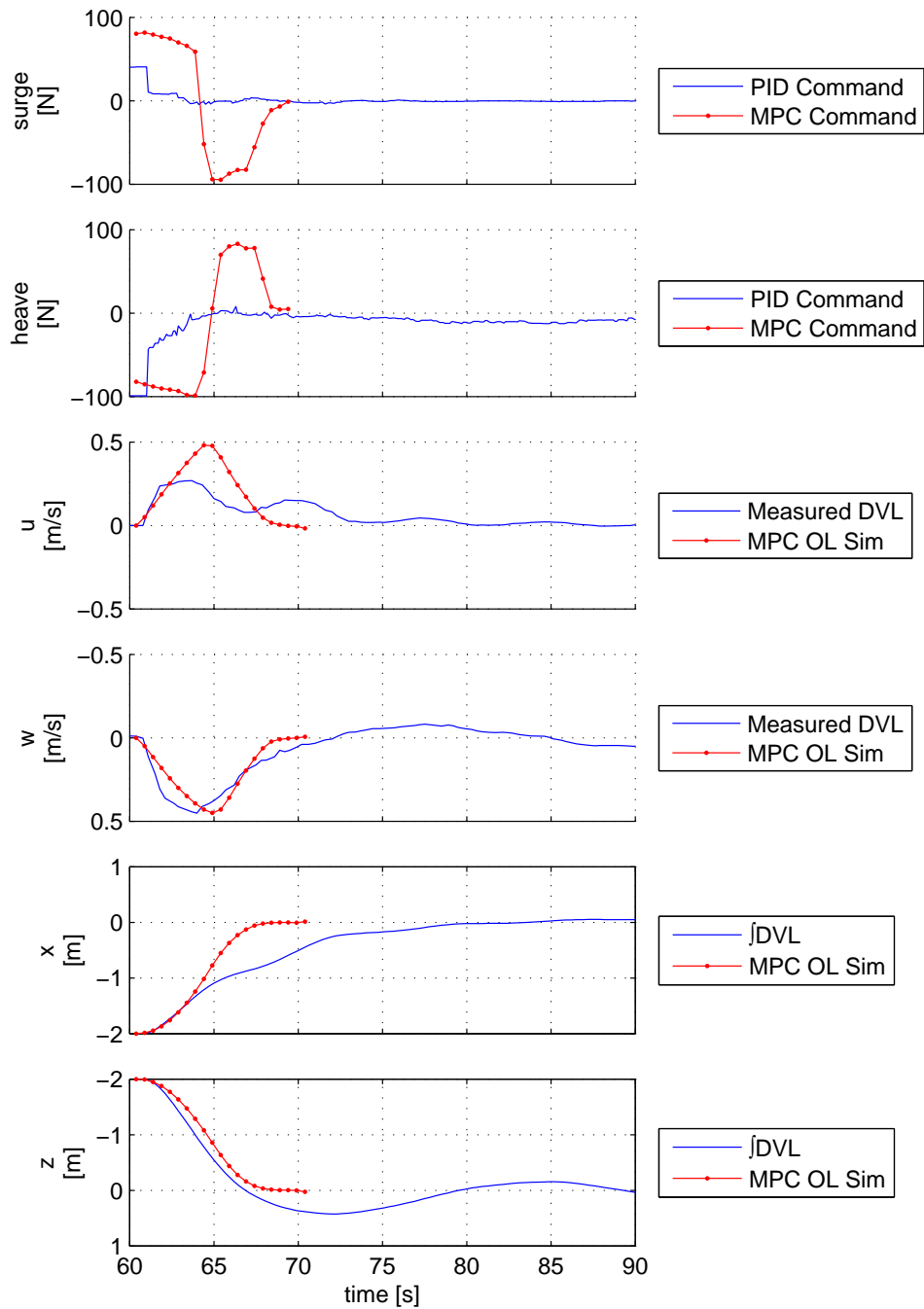


Figure 6-3: Comparison between open-loop MPC simulation and closed-loop PID experiment: Response to step change in desired surge position (+2m) and heave position (-2m). The simulated MPC controller is shown to perform more aggressive maneuvers compared to a traditional PID controller, resulting in faster attainment of the goals. MPC characteristics: $N=20$, $\Delta t=0.5s$. Bound conditions: $u_T=[10(N), 240(N)]$, $u_{\dot{\alpha}}=[-150(\text{deg/s}), 150(\text{deg/s})]$

controller compared to that of the simulation. Note that the bound conditions for the thrusters u_T defined on the figure represent the total thrust for both thrusters, the lower bound is designed to accommodate for predicted deadband, and the upper bound limits response due to operation for safety reasons as experiments were performed in an enclosed testing area. The predicted response of the open-loop MPC controller consists of operating at the upper bounds of the thrust input. The RTU spins accordingly, to get the desired force vector in order to maneuver in 2-DOF simultaneously. The thrust levels off at around 6s.

There was found to be some disconnect between commanded versus actual control inputs (see figure 6-5). MOOS, as implemented on the Odyssey IV, was not designed to accept actuator commands at the update frequency that was desired for these MPC tests. This produces some difference in the performance of the experimental controller. MOOS often receives the desired commands for the MPC controller and records these as “Commanded”. However, the actual “Measured” output from the RTU shows that the actual positions commanded do not match as closely as we would like.

When the model is simulated using the control inputs of MOOS commanded propeller speed and actual measured RTU position, the simulation agrees more closely to measurements. This adds credibility to the model and suggests that errors are primarily due to the disagreement between commanded and actual control inputs within MOOS.

6.3.4 MPC-PID Hybrid

Because of issues from the software side in running experiments, an MPC-PID hybrid solution was developed (Figure 6-6). This solution was hoped to resolve small errors due to mismatch between the MPC-MOOS communication, using the proven PID controller. This MPC-PID hybrid is shown in figure 6-7. A feed-forward MPC solution provides the majority of the controller input. The resulting error between the predicted MPC state is compared with the actual, then the feedback PID controller corrects for any error. The total command is then the vector sum of the PID

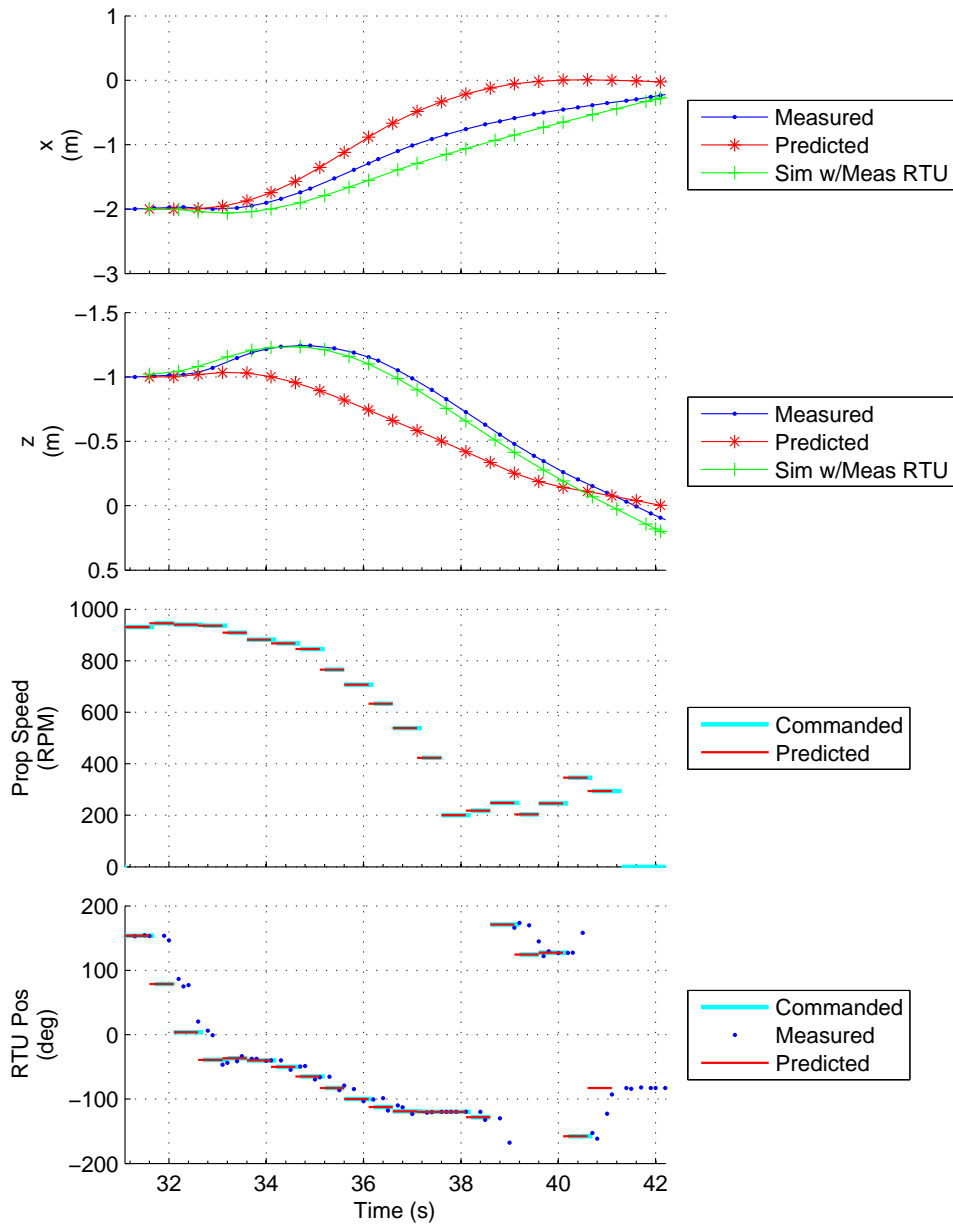


Figure 6-4: Comparison between open-loop MPC simulation and experiment: Response to step change in desired surge position (+2m) and heave position (-1m). The predicted MPC simulation (“Predicted”) is compared with MPC open-loop experiment (“Measured”). The simulation is then re-run with the measured commands from the experiment (“Sim w/ Meas RTU”). MPC characteristics: prediction horizon $N=20$, time step $\Delta t=0.5s$. Bound conditions: $u_T=[10(N), 240(N)]$, $u_{\dot{\alpha}}=[-150(\text{deg/s}), 150(\text{deg/s})]$

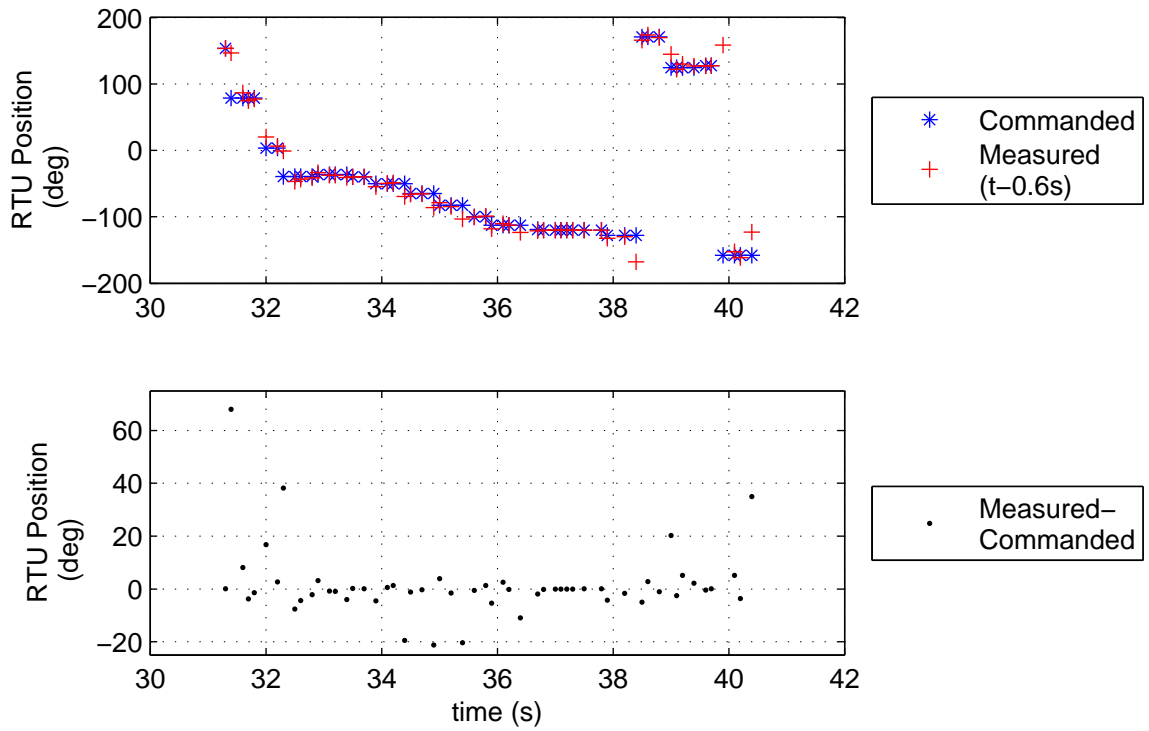


Figure 6-5: Comparison between RTU commands and measured output for figure 6-4. In this figure, the command is delayed by 0.6s in order to accommodate for internal delay. The residual difference between commanded and actual output is largest when large changes in RTU position are commanded.

command and the MPC command, essentially:

$$F_{surge,total} = F_{surge,MPC} + F_{surge,PID} \quad (6.10)$$

$$F_{heave,total} = F_{heave,MPC} + F_{heave,PID} \quad (6.11)$$

Figure 6-7 demonstrates the experimental performance of this hybrid controller.

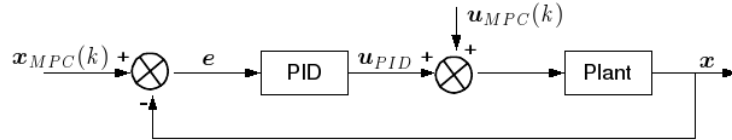


Figure 6-6: MPC-PID hybrid control diagram. For time $t(k) \leq t \leq t(k+1)$, the predicted state $\mathbf{x}_{MPC}(k)$ at discrete time instance k is compared with the actual state \mathbf{x} . This error \mathbf{e} is used to generate the PID control \mathbf{u}_{PID} . The total control applied is then the vector sum of the PID command and MPC command $\mathbf{u}_{MPC}(k)$.

The MPC-PID controller improves performance over the open-loop controller, as the vehicle returns to approximately zero surge velocity at the end of the experiment. There is still some disconnect, however, as the vehicle does not arrive at the desired final position even with the PID feedback control.

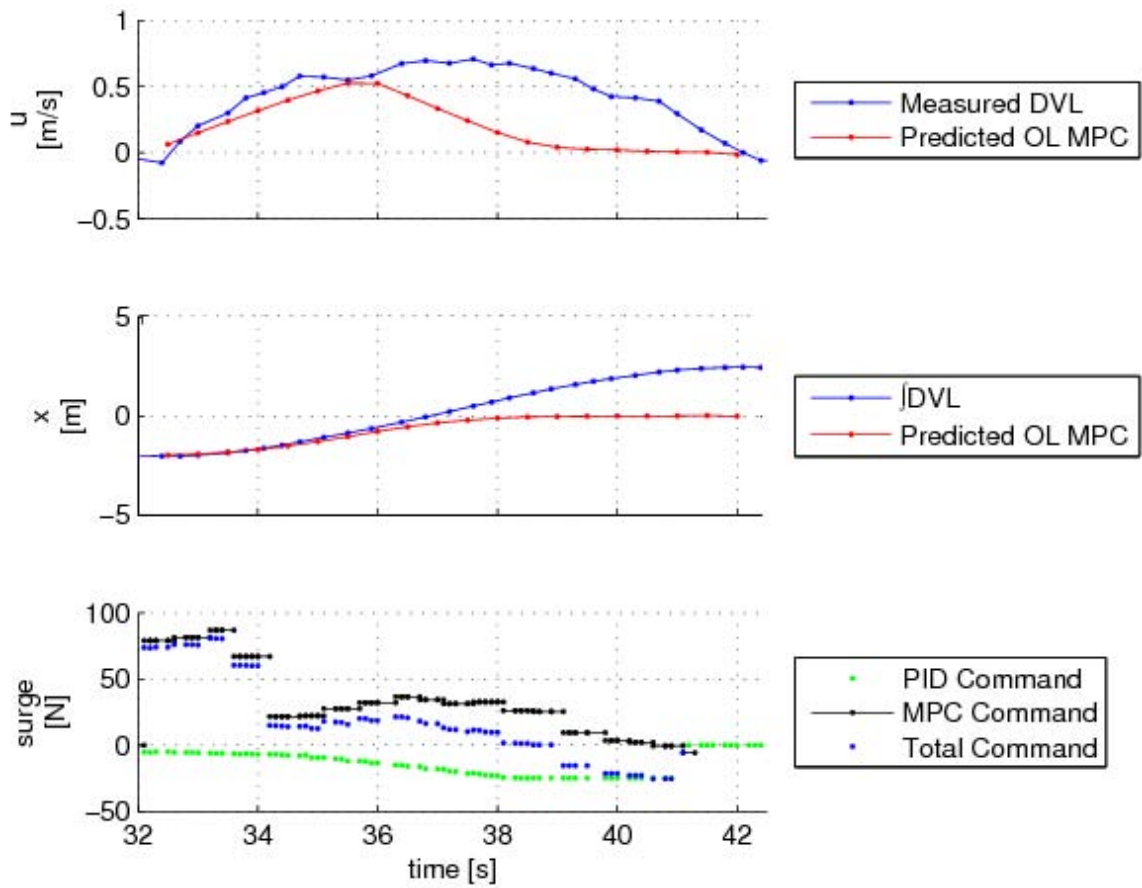


Figure 6-7: MPC-PID hybrid controller performance: Response to step change in desired surge position (+2m) and heave position (-1m). The PID feedback control appears to improve performance, but not on the desired time scale. MPC characteristics: prediction horizon $N=20$, time step $\Delta t=0.5s$. Bound conditions: $u_T=[10(N), 240(N)]$, $u_{\dot{\alpha}}=[-150(\text{deg/s}), 150(\text{deg/s})]$

Chapter 7

Conclusions

This thesis presents the development and analysis of a model of the Odyssey IV AUV. The nonlinear model developed includes rigid body and hydrodynamic effects, using a combination of theoretical and empirical approaches. The model was linearized about time-varying reference trajectories to make the control problem tractable. Analysis of the model suggests decoupling into three lightly-interacting sub-groups. Experiments show good agreement between model prediction of vehicle motions and dynamics. This lends credibility to its use as a good prediction model for model-based control.

Azimuthing propulsion provides improved maneuverability over traditional propulsion systems, even at zero-forward speed. The application of azimuthing propulsion to the Odyssey IV AUV brings additional complexity, as the dynamic response of the actuation is on the same time scale as the vehicle. Unsteady thrust development for azimuthing actuators is not well understood. This thesis presents a simple model for unsteady thrust development that takes into account time-dependence and effect of azimuthing. This approach was shown to improve model performance.

The challenges associated with control of the Odyssey IV AUV involve a complex dynamic model and a nonlinear control problem further complicated by the azimuthing thruster configuration. The current Odyssey IV controller uses PID control. Experimental performance of this controller was analyzed. For complex maneuvers a more advanced controller becomes necessary.

Model predictive control (MPC) was investigated as it has the ability to handle

constraints and nonlinearities. A nonlinear MPC-based controller was developed, and simulations suggest improved performance over the current PID controller. Because it incorporates future knowledge of the system behavior and physical constraints, the MPC-based solution is able to perform more aggressive maneuvers with better usage of the thrusters.

Several algorithms for solving the performance optimization function are analyzed. Computation of the on-line optimization problem is identified as the limiting factor in a real-time MPC-based controller. An experimental open-loop controller was developed, such that the optimization problem was computed off-line and the appropriate control solution for each time step was commanded. Some disconnect was observed between commanded and actual control inputs due to communication issues with the software. A hybrid MPC-PID controller was then proposed, such that a feed-forward MPC solution provides the majority of the controller input, and a feed-back PID controller corrects for any additional error. The same communication problem between commanded versus actual control inputs was observed. Successful implementation of a hybrid PID-MPC controller would require that these errors be resolved. By overcoming these obstacles, results from simulation suggest that a nonlinear MPC-based controller would provide substantial contributions to maneuvering and path-planning.

Appendix A

Vehicle Mass Table

Table A.1: Odyssey IV Detailed Mass Table

Part	Dry (kg)	Displaced (kg)	Wet (kg)	x_G (m)	z_G (m)	x_B (m)	z_B (m)
RTU	32.66	14.81	17.85	0	0	0	0
thruster guards	7.03	1.24	5.8	0	0	0	0
thruster + arm	12.61	5.39	7.22	0	0	0	0
x thruster/mount	12.7	5.35	7.35	0	0	0	0
front sphere	26.31	45.24	-18.93	0.03	-0.02	0.05	-0.04
rear sphere	26.31	45.22	-18.91	-0.02	0.02	-0.04	0.04
battery	34.93	0	34.93	-0.03	0.03	0	0
lifting bale	4.22	0.92	3.3	0	-0.01	0	0
frame rails	15.1	15.88	-0.77	0	0	0	0
frame other pieces	17.24	17.98	-0.75	0	0	0	0
frame metal struts	8.85	0.98	7.86	0	0	0	0
guard bracket	2.54	0.29	2.25	0	0	0	0
electronics	9.53	0	9.53	0.01	-0.01	0	0
frame metal strips	3.27	0.36	2.9	0	0	0	0
bolts	4.08	0.45	3.63	0	0	0	0
cables	4.54	1.36	3.18	0	0	0	0
DVL	9.98	4.73	5.25	-0.01	0.01	0	0
sphere handles	0.91	0.14	0.77	0	0	0	0
rounded fairings	14.33	13.39	0.95	0	0	0	0
side fairings	7.37	6.7	0.67	0	0	0	0
altimeter	1.59	0.45	1.13	0	0	0	0
depth sensor	3.18	0.45	2.72	0	0	0	0
flotation	79.74	159.48	-79.74	0.04	-0.03	0.02	-0.06
Total	339	340.83	-1.84	0.01	0.00	0.02	-0.06

Appendix B

Coefficient Matrix

The equations of motion are linearized about time-varying reference trajectory $\boldsymbol{\nu}_0(t)$, as described in Section 4.2.1:

$$\boldsymbol{\nu}_0 = [u_0, v_0, w_0, p_0, q_0, r_0]^T \quad (\text{B.1})$$

such that the equations of motion can be written as

$$\dot{\boldsymbol{\nu}} = \mathbf{A}\boldsymbol{\nu} + \mathbf{B}\mathbf{u} \quad (\text{B.2})$$

where

$$\mathbf{A} = -\mathbf{M}^{-1}(\mathbf{C} + \mathbf{D}) \quad (\text{B.3})$$

The matrix \mathbf{A} is velocity dependent due to the drag coefficient matrix \mathbf{D} , therefore, we are interested in finding numerical values for \mathbf{A} , for different reference velocities.

For $\boldsymbol{\nu}_0 = [1, 0, 0, 0, 0, 0]^T$:

$$\mathbf{A}_0 = \begin{bmatrix} -1.29\text{e-}01 & 5.30\text{e-}03 & 0 & 0 & -2.69\text{e-}01 & 5.00\text{e-}04 \\ 1.00\text{e-}04 & -6.35\text{e-}02 & 1.00\text{e-}04 & 5.01\text{e-}02 & 1.00\text{e-}04 & -1.91\text{e-}01 \\ 3.82\text{e-}02 & -1.43\text{e-}02 & -5.81\text{e-}01 & -8.80\text{e-}03 & 6.83\text{e-}01 & 0 \\ -8.10\text{e-}03 & 2.09\text{e+}00 & 2.28\text{e-}02 & 1.53\text{e+}00 & 4.22\text{e-}02 & 9.00\text{e-}04 \\ -3.02\text{e-}01 & 9.10\text{e-}03 & -9.92\text{e-}01 & -7.00\text{e-}03 & 9.40\text{e-}02 & 1.00\text{e-}04 \\ -1.00\text{e-}03 & 4.60\text{e-}01 & -1.10\text{e-}03 & -5.00\text{e-}04 & -1.30\text{e-}03 & 4.78\text{e-}02 \end{bmatrix} \quad (\text{B.4})$$

For $\boldsymbol{\nu}_0 = [0, 1, 0, 0, 0, 0]^T$:

$$\mathbf{A} = \begin{bmatrix} 0 & -1.00\text{e-}04 & 0 & -1.70\text{e-}03 & -1.44\text{e+}00 & 0 \\ -2.00\text{e-}04 & 1.20\text{e-}03 & 0 & 2.83\text{e-}01 & 4.00\text{e-}04 & -1.00\text{e-}04 \\ -2.04\text{e-}01 & 7.52\text{e-}02 & -2.92\text{e-}02 & 1.00\text{e-}04 & 0 & -7.80\text{e-}03 \\ 4.33\text{e-}02 & -1.11\text{e+}01 & 2.10\text{e-}03 & -2.70\text{e-}03 & -1.00\text{e-}04 & 1.34\text{e+}00 \\ 1.62\text{e+}00 & -4.20\text{e-}02 & 5.30\text{e-}03 & -4.00\text{e-}04 & 0 & -5.10\text{e-}03 \\ 1.80\text{e-}03 & -1.23\text{e-}02 & 0 & -1.51\text{e-}01 & -3.50\text{e-}03 & 1.50\text{e-}03 \end{bmatrix} \quad (\text{B.5})$$

For $\boldsymbol{\nu}_0 = [1, 1, 0, 0, 0, 0]^T$:

$$\mathbf{A}_0 = \begin{bmatrix} -1.29\text{e-}01 & 5.10\text{e-}03 & 0 & -1.70\text{e-}03 & -1.71\text{e+}00 & 6.00\text{e-}04 \\ -1.00\text{e-}04 & -6.22\text{e-}02 & 1.00\text{e-}04 & 3.33\text{e-}01 & 5.00\text{e-}04 & -1.91\text{e-}01 \\ -1.66\text{e-}01 & 6.09\text{e-}02 & -6.10\text{e-}01 & -8.70\text{e-}03 & 6.83\text{e-}01 & -7.80\text{e-}03 \\ 3.52\text{e-}02 & -9.03\text{e+}00 & 2.49\text{e-}02 & 1.53\text{e+}00 & 4.21\text{e-}02 & 1.34\text{e+}00 \\ 1.31\text{e+}00 & -3.30\text{e-}02 & -9.87\text{e-}01 & -7.40\text{e-}03 & 9.40\text{e-}02 & -5.00\text{e-}03 \\ 8.00\text{e-}04 & 4.47\text{e-}01 & -1.10\text{e-}03 & -1.52\text{e-}01 & -4.80\text{e-}03 & 4.92\text{e-}02 \end{bmatrix} \quad (\text{B.6})$$

Bibliography

- [1] Bluefin robotics corporation. <http://www.bluefinrobotics.com/index.htm>.
- [2] Deep water corals. <http://www.coris.noaa.gov/about/deep/>.
- [3] F-22 raptor. <http://www.lockheedmartin.com/products/f22/index.html>.
- [4] A. P. Aguiar and A. M. Pascoal. Dynamic positioning and way-point tracking of underactuated AUVs in the presence of ocean currents. *International Journal of Control*, 80(7):1092–1108, 2007.
- [5] Abran Alaniz. Model predictive control with application to real-time hardware and guided parafoil. Master’s thesis, Massachusetts Institute of Technology, Cambridge, MA, 2004.
- [6] F. Allgower, T. A. Badgwell, S. J. Qin, J. B. Rawlings, and S. J. Wright. Nonlinear predictive control and moving horizon estimation – an introductory overview. In P. M. Frank, editor, *Advances in Control, Highlights of ECC’99*, pages 391–449. Springer, 1999.
- [7] F. Allgower, R. Findeisen, and Z. K. Nagy. Nonlinear model predictive control: From theory to application. *Journal of the Chinese Institute of Chemical Engineers*, 35(3):299–315, May 2004.
- [8] Juan Jost Arrieta-Camacho and Lorenz T. Biegler. Real time optimal guidance of low-thrust spacecraft - an application of nonlinear model predictive control. In E. Belbruno, editor, *New Trends in Astrodynamics and Applications*, volume 1065 of *Annals of the New York Academy of Sciences*, pages 174–188. 2005.
- [9] A. Bemporad, M. Morari, V. Dua, and E. N. Pistikopoulos. The explicit linear quadratic regulator for constrained systems. *Automatica*, 39(10):1845–1846, October 2003.
- [10] Louis Scott Breger. *Control of spacecraft in proximity orbits*. PhD thesis, Massachusetts Institute of Technology, Cambridge, MA, 2007.
- [11] W. H. Chen, D. J. Ballance, and J. O’Reilly. Model predictive control of nonlinear systems: Computational burden and stability. *IEE Proceedings-Control Theory and Applications*, 147(4):387–394, July 2000.

- [12] T. F. Coleman and Y. Y. Li. An interior trust region approach for nonlinear minimization subject to bounds. *SIAM Journal on Optimization*, 6(2):418–445, May 1996.
- [13] P. J. Craven, R. Sutton, and R. S. Burns. Control strategies for unmanned underwater vehicles. *Journal of Navigation*, 51(1):79–105, January 1998.
- [14] R Damus. Systematic coverage and inspection of underwater archaeological sites using AUVs. Technical Report SG04-02, MIT Sea Grant, August 2004.
- [15] John D’Errico. <http://www.mathworks.com/matlabcentral/fileexchange/8277>.
- [16] S Desset, C Chrysostomidis, R Damus, F Hover, J Morash, and V Polidoro. Closer to deep underwater science with odyssey iv class hovering autonomous underwater vehicle. In *OCEANS*, pages 2129–2134. MTS/IEEE, 2005.
- [17] M. Diehl, R. Findeisen, F. Allgower, H. G. Bock, and J. P. Schloder. Nominal stability of real-time iteration scheme for nonlinear model predictive control. *IEE Proceedings-Control Theory and Applications*, 152(3):296–308, May 2005.
- [18] William B. Dunbar, M. B. Milam, R. Franz, and R. M. Murray. Model predictive control of a thrust vectored flight control experiment. In *IFAC World Congress*, Barcelona, Spain, 2002.
- [19] Justin Eskesen. SGM00S. <http://scripts.mit.edu/jge/auvwiki/index.php?title=SGMOOS>.
- [20] Jonathan Evans, Paul Redmond, Costas Plakas, Kelvin Hamilton, and David Lane. Autonomous docking for intervention-AUVs using sonar and video-based real-time 3D pose estimation. *OCEANS 2003. Proceedings*, Sept 2003.
- [21] H. J. Ferreau, H. G. Bock, and M. Diehl. An online active set strategy to overcome the limitations of explicit MPC. *International Journal of Robust and Nonlinear Control*, 18(8):816–830, May 2008.
- [22] R. Findeisen and F. Allgower. An introduction to nonlinear model predictive control. In *Proc. 21st Benelux Meeting on Systems and Control*, Veldhoven, Netherlands, 2002.
- [23] R. Findeisen and F. Allgower. Computational delay in nonlinear model predictive control. In *Proc. Int. Symp. Advance Control of Chemical Processes*, 2004.
- [24] Thor I Fossen. *Guidance and Control of Ocean Vehicles*. John Wiley & Sons, New York, 1994.
- [25] R. Franz, M. B. Milam, and J. E. Hauser. Applied receding horizon control of the Caltech ducted fan. In *Proc. American Control Conference*, 2002.
- [26] C. E. Garcia, D. M. Prett, and M Morari. Model predictive control - theory and practice - a survey. *Automatica*, 25(3):335–348, May 1989.

- [27] Matthew B. Greytak. High performance path following for marine vehicles using azimuthing podded propulsion. Master's thesis, Massachusetts Institute of Technology, Cambridge, MA, 2006.
- [28] A. J. Healey and D. Lienard. Multivariable sliding mode control for autonomous diving and steering of unmanned underwater vehicles. *IEEE Journal of Oceanic Engineering*, 18(3):327–339, July 1993.
- [29] A. J. Healey, S. M. Rock, S. Cody, D. Miles, and J.P. Brown. Toward an improved understanding of thruster dynamics for underwater vehicles. *Autonomous Underwater Vehicle Technology, 1994. AUV '94., Proceedings of the 1994 Symposium on*, pages 340–352, Jul 1994.
- [30] M. A. Henson. Nonlinear model predictive control: current status and future directions. *Computers & Chemical Engineering*, 23(2):187–202, December 1998.
- [31] Sighard F. Hoerner. *Fluid Dynamic Drag*. Hoerner Fluid Dynamics, Bakersfield, CA, 2nd edition, 1965.
- [32] Sighard F. Hoerner. *Fluid Dynamic Lift*. Hoerner Fluid Dynamics, Bakersfield, CA, 2nd edition, 1985.
- [33] Franz S. Hover. Linearized hovering control with one or more azimuthing thrusters. In *Proceedings of the International Conference on Marine Research and Transportation*, Sept 2005.
- [34] K. Ishii, T. Fujii, and T. Ura. An online adaptation method in a neural-network-based control-system for AUVs. *IEEE Journal of Oceanic Engineering*, 20(3):221–228, July 1995.
- [35] Ali Jadbabaie. *Receding Horizon Control of Nonlinear Systems: A Control Lyapunov Function Approach*. PhD thesis, California Institute of Technology, Pasadena, CA, 2000.
- [36] Michael V. Jakuba. Modeling and control of an autonomous underwater vehicle with combined foil/thruster actuators. Master's thesis, Massachusetts Institute of Technology, Cambridge, MA, February 2003.
- [37] M. Kwiesielewicz, W. Piotrowski, and Sutton R. Predictive versus fuzzy control of an autonomous underwater vehicle. In *Proc of IEEE International Conference on Methods and Models in Automation and Robotics*, pages 609–612, Miedzydroje, Poland, August 2001.
- [38] J. C. Lagarias, J. A. Reeds, M. H. Wright, and P. E. Wright. Convergence properties of the Nelder-Mead simplex method in low dimensions. *SIAM Journal on Optimization*, 9(1):112–147, December 1998.

- [39] Tiffany Rae Lapp. Guidance and control using model predictive control for low altitude real-time terrain following flight. Master's thesis, Massachusetts Institute of Technology, Cambridge, MA, 2004.
- [40] Y. G. Le Page and K. W. Holappa. Simulation and control of an autonomous underwater vehicle equipped with a vectored thruster. In *OCEANS*, volume 3, pages 2129–2134, Providence, RI, September 2000. MTS/IEEE.
- [41] N.E. Leonard. Control synthesis and adaptation for an underactuated autonomous underwater vehicle. *IEEE Journal of Oceanic Engineering*, 20(3):211–220, July 1995.
- [42] E V Lewis. *Principles of Naval Architecture*. Society of Naval Architects and Marine Engineers, New Jersey, 1989.
- [43] C. C. Liang and W. H. Cheng. The optimum control of thruster system for dynamically positioned vessels. *Ocean Engineering*, 31(1):97–110, January 2004.
- [44] J. M. Maciejowski, P. J. Goulart, and E. C. Kerrigan. Constrained control using model predictive control. In *Advanced Strategies in Control Systems with Input and Output Constraints*, volume 346 of *Lecture Notes in Control and Information Sciences*, pages 273–291. 2007.
- [45] D. Q. Mayne and H. Michalska. Receding horizon control of nonlinear-systems. *IEEE Transactions on Automatic Control*, 35(7):814–824, July 1990.
- [46] D. Q. Mayne, J. B. Rawlings, C. V. Rao, and P. O. M. Scokaert. Constrained model predictive control: Stability and optimality. *Automatica*, 36(6):789–814, June 2000.
- [47] Anirban Mazumdar. Maneuverability and heading control of compliant biomimetic swimming devices. Bachelor's thesis, Massachusetts Institute of Technology, Cambridge, MA, 2007.
- [48] J Meza and R Oliva. Opt++: An object-oriented toolkit for nonlinear optimization. *ACM Trans. Math. Softw.*, June 2007.
- [49] J. Meza, R. Oliva, P. Hough, and P. Williams. Opt++: An object-oriented toolkit for nonlinear optimization. *ACM Transactions on Math*, 2007.
- [50] Oh M.H. and Oh J.H. Homing and docking control of AUV using model predictive control. In *The Proceedings of the Fifth ISCPE Pacific/Asia Offshore Mechanics Symposium*, pages 130–142, Daejeon, Korea, November 2002.
- [51] M. B. Milam, R. Franz, J. E. Hauser, and R. M. Murray. Receding horizon control of vectored thrust flight experiment. *IEE Proceedings-Control Theory and Applications*, 152(3):340–348, May 2005.

- [52] M. B. Milam and R. M. Murray. A testbed for nonlinear flight control techniques: the Caltech ducted fan. In *Proc. Conference on Control Applications*, 1999.
- [53] Naoki Mizuno, Masaki Kuroda, Tadatsugi Okazaki, and Kohei Ohtsu. Minimum time ship maneuvering method using neural network and nonlinear model predictive compensator. *Control Engineering Practice*, 15(6):757–765, June 2007.
- [54] M. Morari and J. H. Lee. Model predictive control: past, present and future. *Computers & Chemical Engineering*, 23(4-5):667–682, May 1999.
- [55] R. M. Murray and S. S. Sastry. Nonholonomic motion planning - steering using sinusoids. *IEEE Transactions on Automatic Control*, 38(5):700–716, May 1993.
- [56] W. Naeem, R. Sutton, J. Chudley, F. R. Dalglish, and S. Tetlow. A genetic algorithm-based model predictive control autopilot design and its implementation in an autonomous underwater vehicle. *IMEchE Transactions Part M, Journal of Engineering for the Maritime Environment*, 218:175, 2004.
- [57] W. Naeem, R. Sutton, J. Chudley, F. R. Dalglish, and S. Tetlow. An online genetic algorithm based model predictive control autopilot design with experimental verification. *International Journal of Control*, 78(14):1076–1090, September 2005.
- [58] J. N. Newman. *Marine Hydrodynamics*. MIT Press, August 1977.
- [59] Paul Newman. The MOOS. <http://www.robots.ox.ac.uk/~pnewman/TheMOOS/>.
- [60] N. S. Nise. *Control Systems Engineering*. Addison-Wesley, 3rd edition, 2003.
- [61] Katsuhiko Ogata. *Modern Control Engineering*. Prentice Hall, New York, 4th edition, 2001.
- [62] K. Y. Pettersen and O. Egeland. Time-varying exponential stabilization of the position and attitude of an underactuated autonomous underwater vehicle. *IEEE Transactions on Automatic Control*, 44(1):112–115, January 1999.
- [63] William H. Press, Saul A. Teukolsky, William T. Vetterling, and Brian P. Flannery. *Numerical Recipes in C++: The Art of Scientific Computing*. Cambridge University Press, 2002.
- [64] Timothy Jason Prester. Verification of a six-degree of freedom simulation model for the REMUS autonomous underwater vehicle. Master’s thesis, Massachusetts Institute of Technology, Cambridge, MA, 2001.
- [65] S Qin and T Badgwell. *An overview of nonlinear model predictive control applications*. 2000.

- [66] S. J. Qin and T. A. Badgwell. An overview of industrial model predictive control technology. In J. C. Kantor, C. E. Garcia, and B. Carnahan, editors, *Proc. Fifth International Conference on Chemical Process Control*, pages 232–256. American Institute of Chemical Engineers, 1996.
- [67] C. V. Rao, S. J. Wright, and J. B. Rawlings. Application of interior-point methods to model predictive control. *Journal of Optimization Theory and Applications*, 99(3):723–757, December 1998.
- [68] J. B. Rawlings. Tutorial overview of model predictive control. *IEEE Control Systems Magazine*, 20(3):38–52, June 2000.
- [69] Arthur George Richards. Robust constrained model predictive control. Master’s thesis, Massachusetts Institute of Technology, Cambridge, MA, 2002.
- [70] Jeffery Riedel and Anthony Healey. Model based predictive control of auvs for station keeping in a shallow water environment. 2005.
- [71] Alex Rogers. The biology, ecology and vulnerability of deep-water coral reefs. *British Antarctic Survey*, 2004.
- [72] J.-J. E. Slotine and W. Li. *Applied Nonlinear Control*. Prentice Hall, 1991.
- [73] O Sordalen. Optimal thrust allocation for marine vessels. *Control Eng. Practice*, 1997.
- [74] Jeffrey W. Stettler. *Steady and Unsteady Dynamics of an Azimuthing Podded Propulsor Related to Vehicle Maneuvering*. PhD thesis, Massachusetts Institute of Technology, Cambridge, MA, June 2004.
- [75] F. C. Thomas and Y. Y. Li. On the convergence of interior-reflective Newton methods for nonlinear minimization subject to bounds. *Mathematical Programming*, 67(2):189–224, November 1994.
- [76] M. S. Triantafyllou and F. S. Hover. Maneuvering and control of surface and underwater vehicles. MIT Course 2.154 Class Notes, 2000.
- [77] Q. Truong, L. Wang, and P. Gawthrop. Intermittent model predictive control of an autonomous underwater vehicle. In L. Xie, editor, *Proc. Ninth International Conference on Control, Automation, Robotics and Vision*, Singapore, 2006.
- [78] S. Valluri and M. Soroush. A non-linear controller design method for processes with saturating actuators. *International Journal of Control*, 76(7):698–716, May 2003.
- [79] M. J. Van Nieuwstadt and R. M. Murray. Rapid hover-to-forward-flight transitions for a thrust-vectoring aircraft. *Journal of Guidance Control and Dynamics*, 21(1):93–100, January 1998.

- [80] Ding Wang. *Autonomous Underwater Vehicle (AUV) Path Planning and Adaptive On-board Routing for Adaptive Rapid Environmental Assessment*. PhD thesis, Massachusetts Institute of Technology, Cambridge, MA, September 2007.
- [81] Adrian Wills and William Heath. *Interior-Point Algorithms for Nonlinear Model Predictive Control*. Springer Berlin / Heidelberg, 2007.
- [82] M. H. Wright. The interior-point revolution in optimization: History, recent developments, and lasting consequences. *Bulletin of the American Mathematical Society*, 42(1):39–56, 2005.
- [83] Dana R. Yoerger, John G. Cooke, and Jean-Jacques E. Slotine. The influence of thruster dynamics on underwater vehicle behavior and their incorporation into control system design. *IEEE Journal of Oceanic Engineering*, 15(3):167–178, July 1990.
- [84] J. Yu, A. Jadbabaie, J. Primbs, and Y. Huang. Comparison of nonlinear control design techniques on a model of the Caltech ducted fan. *Automatica*, 37(12):1971–1978, December 2001.
- [85] J. Yuh. Design and control of autonomous underwater robots: A survey. *Autonomous Robots*, 9(2):199, September 2000.